A parametric study of the influence of ion and electron properties on the excitation of electromagnetic ion cyclotron waves in coronal mass ejections

Sergio Dasso[1]

Instituto de Física del Plasma, Departamento de Física, Facultad de Ciencias Exactas y Naturales, Universidad de Buenos Aires-Consejo Nacional de Investigaciones Científicas y Técnicas, Buenos Aires, Argentina

Fausto T. Gratton

Instituto de Física del Plasma, Departamento de Física, Facultad de Ciencias Exactas y Naturales, Universidad de Buenos Aires-Consejo Nacional de Investigaciones Científicas y Técnicas, Buenos Aires, Argentina

Charles J. Farrugia

Institute for the Study of Earth, Oceans, and Space, Space Science Center, University of New Hampshire, Durham, New Hampshire, USA

Received 25 June 2002; revised 18 November 2002; accepted 16 January 2003; published 8 April 2003.

[1] Interplanetary coronal mass ejections (ICMEs) often possess a negative proton thermal anisotropy, $A_p = T_{\perp,p}/T_{\parallel,p} - 1 < 0$ ($T_\parallel$, $T_\perp$: parallel and perpendicular temperatures, respectively) so that right-hand polarized electromagnetic ion cyclotron waves (EICWs) may be amplified by a kinetic instability [*Farrugia et al.*, 1998a]. However, in view of the low proton beta of ICMEs, several physical parameters, besides A_p, need to be in the right range to excite this instability with significant growth rates. In this paper we present a parametric study of EICWs aimed at identifying those parameters which are most influential in fostering the emission of these waves in ICME scenarios. We analyze here the influence of: (1) thermal and suprathermal protons, (2) thermal alpha particles (αs), and (3) thermal electrons. We solve the dispersion relation of EICWs including protons, αs and electrons, all modeled with bi-Maxwellian distribution functions, and a minority population of suprathermal protons using a kappa function for the velocity component along the field. For physical regimes of ICMEs we find that the instability depends critically on the values of the following parameters: proton beta, proton thermal anisotropy, relative abundance of the suprathermal protons, α-to-proton relative abundance, α-to-proton temperature ratio, α particle thermal anisotropy, electron-to-proton temperature ratio, and thermal anisotropy of electrons. The effect of these parameters on the instability is either direct (when they increase the number of resonant particles) or indirect (when they decrease the phase speed of the wave so that more particles can resonate). Data surveys on EICWs should take into account the whole set of parameters indicated here, since the expected level of wave excitation results from their combined action. The study may be useful in understanding the considerable level of magnetic fluctuations observed in interplanetary CMEs by the Wind spacecraft. *INDEX TERMS:* 2111 Interplanetary Physics: Ejecta, driver gases, and magnetic clouds; 7867 Space Plasma Physics: Wave/particle interactions; 2164 Interplanetary Physics: Solar wind plasma; 7871 Space Plasma Physics: Waves and instabilities; 7827 Space Plasma Physics: Kinetic and MHD theory; *KEYWORDS:* interplanetary coronal mass ejections, magnetic clouds, plasma waves, kinetic instabilities, ion-cyclotron instability, thermal anisotropy

Citation: Dasso, S., F. T. Gratton, and C. J. Farrugia, A parametric study of the influence of ion and electron properties on the excitation of electromagnetic ion cyclotron waves in coronal mass ejections, *J. Geophys. Res.*, *108*(A4), 1149, doi:10.1029/2002JA009558, 2003.

1. Introduction

[2] Coronal mass ejections (CMEs) represent gigantic expulsions of mass and magnetic flux from the Sun. When observed in the interplanetary medium these objects are often called ''interplanetary manifestations of CMEs''

[1]Now at Instituto de Astronomía y Física del Espacio, Departamento de Física, Facultad de Ciencias Exactas y Naturales, Universidad de Buenos Aires-Consejo Nacional de Investigaciones Científicas y Técnicas, Buenos Aires, Argentina.

0148-0227/03/2002JA009558

(ICMEs). ICMEs are characterized by a number of field and plasma properties. Chief among these are: (1) low proton temperatures, T_p [see, e.g., *Richardson and Cane*, 1995, and references therein]; (2) bi-directional flows (along the field lines) of suprathermal (energy E > 80 eV) electron fluxes [*Montgomery et al.*, 1974; *Bame et al.*, 1981; *Gosling et al.*, 1987]; (3) bi-directional flows along the field lines of suprathermal protons, of energies in the few keV to ~1 MeV range [*Gosling et al.*, 1981; *Marsden et al.*, 1987; *Galvin et al.*, 1987]; (4) a relative α particle-to-proton density ratio which is highly variable and may be very different from the typical 4% observed in the solar wind; and (5) electron temperatures, T_e, which are frequently higher than proton temperatures (T_p) [*Osherovich et al.*, 1993; *Richardson et al.*, 1997]. The important subset of ICMEs known as interplanetary magnetic clouds is distinguished by enhanced magnetic field strengths with respect to ambient values, a large rotation of the magnetic field vector, and low T_p [*Burlaga et al.*, 1981; *Burlaga*, 1995]. The majority of the ICMEs have $T_\parallel > T_\perp$, where $\parallel$ and $\perp$ denote directions parallel and perpendicular to the magnetic field [*Zwickl et al.*, 1983; *Gosling et al.*, 1987; *Galvin et al.*, 1987]. Electrons have been noted to show a similar trend [*Pillipp et al.*, 1987; *Gosling et al.*, 1987]. For a review on ICMEs, see *Gosling* [1990] and *Neugebauer and Goldstein* [1997], and for a review on magnetic clouds, see *Osherovich and Burlaga* [1997].

[3] Since the proton thermal anisotropy, $A_p = T_{p,\perp}/T_{p,\parallel} - 1$, is frequently observed to be negative, ICMEs may develop the kinetic instability of electromagnetic ion cyclotron waves (EICWs) corresponding to the right-hand (RH) polarized branch of the low frequency dispersion relation. The possibility that RH-EICWs may be excited in ICMEs, as a consequence of $A_p < 0$ was first considered by *Farrugia et al.* [1998a]. Preliminary examinations of the influence of the thermal properties of protons and α particles, on the EICW instability for ICMEs conditions was given by *Dasso et al.* [1999] and *Dasso et al.* [2002]. Explorative analysis of effects of hot and anisotropic electrons have been developed in *Gratton et al.* [1998] and *Dasso et al.* [2000]. In particular, an exploration of the necessary conditions for the development of EICWs inside the ICME observed by Wind on August 7–8, 1996, was studied by *Dasso et al.* [2001].

[4] This paper addresses RH waves in the range of the cyclotron frequency in solar ejecta, which correspond to ~1 Hz in the spacecraft frame at 1AU. In particular, it is the purpose of our study to show that, with respect to the rates predicted by the mere consideration of A_p and β_p, the growth rates of RH-EICWs can be considerably enhanced, when the values of other parameters mentioned above fall into certain ranges which might be observed in ICMEs. Some of the parameters bearing on EICW growth are not routinely measured. For this reason, we shall carry out here a parameter study, where each relevant parameter is varied around a nominal value. We also study the effect of thermal and suprathermal proton properties on the instability of EICWs. We examine first the influence of the thermal properties of protons, modeling the distribution function (f_p) as a bi-Maxwellian. Next we consider the effect of suprathermal particles, comparing the intensity of the wave emission for proton distribution functions with, and without, energetic components. We focus attention on suprathermal wings along the background field B_0, modelling f_p as the sum of two components, a bi-Maxwellian core and a minority population (with density n_m) represented as the product of a κappa function for the parallel velocity $v_\parallel$, and a Maxwellian function for the perpendicular velocity, $v_\perp$. For the distribution function of the α particles we consider only bi-Maxwellians because the suprathermal properties of αs in ICMEs are not well known. We study the influence on the waves of three α parameters, $A_\alpha = T_{\alpha,\perp}/T_{\alpha,\parallel} - 1$, T_α/T_p, and abundance ratio, $\eta_\alpha = n_\alpha/n_p$. We model the distribution function of the electrons (f_e) with bi-Maxwellians also. We examine the influence of T_e/T_p and A_e on the wave excitation.

[5] The list of input parameters that define the distribution functions of ions (core protons, energetic protons modeled by a κappa distribution function, and alpha particles) and electrons are $n_p, T_{\parallel,p}, T_{\perp,p}, \kappa, n_m, T_{\parallel,m}, T_{\perp,m}, n_\alpha, T_{\parallel,\alpha}, T_{\parallel,\alpha}, T_{\perp,\alpha}, T_{\parallel,e}, T_{\perp,e}$.

[6] We analyze the growth rate sensitivity to variations of the most important parameters. Since the amplification of the waves depends on a combination of factors, we consider the variation of each key parameter separately from the others, to acquire a deeper insight into the mechanisms that control this instability. From the theory, then, we determine the physical conditions that lead to significant wave emission rates in ICMEs.

[7] The layout of the paper is as follows. In a theoretical section we derive the dispersion relation of right-hand polarized EICW. In section 3 we give the results for growth and damping rates, unstable frequency intervals, obtained from numerical solutions of the dispersion relation, as well as approximate formulas for the maximum growth rate dependence on key parameters. A final section gives a discussion and our conclusions.

2. Dispersion Relations for EICWs

[8] We study the linear stage of the resonant instability of right-hand (RH) polarized EICWs propagating parallel to the magnetic field which is due to negative thermal anisotropy of ions. The resonant instability of EICWs (both for right and left handed polarization) in space physics was studied by *Kennel and Scarf* [1968], in one of the earliest papers on this topic. There is now a large literature on this subject, and surveys of its relevance for space physics can be found, e.g., in the work of *Gary* [1993], or of *Treumann and Baumjohann* [1997].

2.1. Bi-Maxwellian Plasma Components

[9] The dispersion relation for RH polarized EICWs can be written as

$$k^2c^2 = \omega^2\epsilon_R \tag{1}$$

where ϵ_R is the component of the dielectric tensor corresponding to the right-hand polarization. It is defined by the following equation, derived from plasma kinetic theory [see, e.g., *Stix*, 1992; *Gary*, 1993],

$$\epsilon_R = 1 + \sum_s \frac{\omega_{ps}^2}{\omega^2}\left[A + \frac{(A+1)\omega + A\Omega}{kw_\parallel} Z\left(\frac{\omega+\Omega}{kw_\parallel}\right)\right]_s, \tag{2}$$

[10] The sum extends over all species, (electrons, protons, and αs); ω is the complex angular frequency of the wave [$\omega = \omega_r + i\gamma$]; k is the wave number parallel to the ambient magnetic field and Z is the plasma Zeta function. In (1), all species are modeled by bi-Maxwellian distribution functions. In the same expression, ω_{ps} and ω_s are the plasma and cyclotron frequencies, respectively; $w_{\|,s} = \sqrt{2T_{\|,s}/m_s}$, is the thermal speed (temperature in energy units; and m_s mass of the particle); $A_s = T_{\perp,s}/T_{\|,s} - 1$, is the thermal anisotropy; c is the speed of light. Wave quantities vary as $\exp[i(kz - \omega t)]$, where the z axis is aligned along the magnetic field.

[11] In the following, we normalize frequencies and growth rates with the proton cyclotron frequency: $x = x_r + ig = (\omega_r + i\gamma)/\Omega_p$, where $\Omega_p = eB_0/m_p c$ is the proton cyclotron frequency and B_0 is the background magnetic field. The dimensionless wave number is $y = kV_A/\Omega_p$, where $V_A = B_0/\sqrt{4\pi n_p m_p}$ is the proton Alfvén velocity. For a plasma consisting of protons, αs, and electrons, and using dimensionless quantities equation (1) can be written as

$$y^2 = A_p + \frac{A_p(x+1)+x}{y\beta_{\|,p}^{1/2}} Z\left(\frac{x+1}{y\beta_{\|,p}^{1/2}}\right) + \eta_\alpha A_\alpha + \eta_\alpha \frac{A_\alpha(x+1/2)+x}{y\beta_{\|,\alpha}^{1/2}} Z\left(\frac{x+1/2}{y\beta_{\|,\alpha}^{1/2}}\right) + A_e\eta_e\mu^{-1} + \eta_e^{3/2}\mu^{-1/2}\frac{A_e(x-\mu^{-1})+x}{y\beta_{\|,e}^{1/2}} Z\left(\frac{x-\mu^{-1}}{y\beta_{\|,e}^{1/2}}\eta_e^{1/2}\mu^{1/2}\right) \quad (3)$$

[12] The following dimensionless parameters have been introduced: $\beta_{\|,p} = \beta_p/(\frac{2}{3}A_p + 1)$ (with $\beta_p = 8\pi n_p T_p/B_0^2$), $\beta_{\|,\alpha} = \beta_p\,(T_\alpha/4T_p)/(\frac{2}{3}A_\alpha + 1)$, $\beta_{\|,e} = 8\pi n_e T_{\|,e}/B_0^2 = \beta_p\eta_e\,(T_e/T_p)/(\frac{2}{3}A_e + 1)$, $\eta_\alpha = n_\alpha/n_p$, $\eta_e = n_e/n_p$, and $\mu = m_e/m_p$.

[13] A survey of the literature allows us to collect a set of observed physical properties of ICMEs, from which we propose several possible parameter scenarios for the wave theory. For those parameters insufficiently known from observations, we complement the information with educated guesses.

[14] Values of β_p have been chosen between 0.1 and 0.6 [*Richardson and Cane*, 1995, and references therein]. In particular, interplanetary magnetic clouds, often have extremely low β_ps, although from time to time values up to $\beta_p \sim 0.4$ have also been observed in parts of the ejecta [*Farrugia et al.*, 1998b; *Dasso et al.*, 2001]. The proton anisotropy, A_p, is very important not only because it indicates the amount of free energy that drives the instability, but also because the quantity that characterizes the proton emission intensity is not β_p directly but rather $\beta_{p,\|}$. The latter is larger than β_p for $A_p < 0$. We reach values of $T_\|/T_\perp$ as high as $T_\|/T_\perp \sim 5$ (i.e. $A_p \sim -0.8$) [*Gosling et al.*, 1987]. In fact, magnetic clouds with even higher thermal anisotropies have been occasionally observed ($T_\|/T_\perp \sim 10$ [*Galvin et al.*, 1987]).

[15] The abundance of αs relative to protons in ICMEs is frequently larger than typical solar wind values of $\sim$3–4% [*Schwenn*, 1990, and references therein]. The relative abundance η_α is highly variable in different ICMEs, ranging from 1% to more than 20% [e.g., *Gosling et al.*, 1987; *Galvin*, 1997]. Quantity η_α, too may vary greatly inside the same ICME and values of order $\eta_\alpha \sim 0.15$, or greater, have sometimes been reported [e.g., *Borrini et al.*, 1982; *Zwickl et al.*, 1983]. In the solar wind the thermal velocities of αs and protons are similar, so that the temperature ratio $T_\alpha/T_p \sim 2$–4 [*Marsch*, 1991]. However, in ICMEs T_α/T_p may be very different from 4. Part of magnetic clouds with T_α/T_p as high as 36 have been observed [*Burlaga et al.*, 1998]. However, despite some published studies, there are as yet no systematic studies of T_α/T_p for ICMEs, and we shall accordingly vary this parameter. Thermal anisotropy of alpha particles is very poorly known quantity and we shall take $A_\alpha \sim A_p$. Nevertheless, we shall also study variations of this parameter.

[16] Quantity T_e is generally larger than the T_p [*Gosling et al.*, 1987; *Galvin et al.*, 1987; *Pillipp et al.*, 1987]. In particular, in the statistical study by *Richardson et al.* [1997] it has been suggested that $T_e/T_p > 2$ is a criterion to identify ICMEs. On occasion, T_e/T_p reaches values as high as 7–10 [*Osherovich et al.*, 1993]. The parallel temperature of electrons is generally greater than the perpendicular temperature, $T_{e,\|} > T_{e,\perp}$, so that we can assume $A_e < 0$ in our numerical analysis [*Gosling et al.*, 1987; *Galvin et al.*, 1987; *Pillipp et al.*, 1987; *Dasso et al.*, 2001].

[17] When $\gamma \ll \omega_r$, an approximation for γ is given by

$$\gamma \simeq -\frac{\omega_r \Im(\epsilon_R)}{\frac{\partial}{\partial\omega_r}\left(\Re\left(\omega_r^2\epsilon_R\right)\right)},$$

where information on ω_r (k) is needed and may be obtained by solving the companion equation

$$k^2c^2 = \omega_r^2\Re(\epsilon_R)$$

[18] Expanding the plasma Z functions in equation (3), one obtains the following expression for the normalized growth rate, $g = g_p + g_\alpha$, where the contributions to g of protons and αs are given, approximately, by

$$g_p = -\sqrt{\pi}\frac{\left[(A_p+1)x_r + A_p\right]\exp\left[-\frac{(x_r+1)^2}{y^2\beta_{\|,p}}\right]/\beta_{\|,p}^{1/2}}{y\left[2x_rV_A^2/c^2 - 1/(1+x_r)^2 - \eta_\alpha/2(x_r+1/2)^2 + 1 + 2\eta_\alpha\right]} \quad (4)$$

and

$$g_\alpha = -\eta_\alpha\sqrt{\pi}\frac{\left[(A_\alpha+1)x_r + A_\alpha/2\right]\exp\left[-\frac{(x_r+1/2)^2}{y^2\beta_{\|,\alpha}}\right]/\beta_{\|,\alpha}^{1/2}}{y\left[2x_rV_A^2/c^2 - 1/(1+x_r)^2 - \eta_\alpha/2(x_r+1/2)^2 + 1 + 2\eta_\alpha\right]} \quad (5)$$

[19] Electrons with velocities in resonance with the EICWs are in the far tails of the bi-Maxwellian distribution, and therefore the corresponding term g_e is neglected here (but see section 3.3 on their influence on g via an indirect effect). Note that the denominators of equations (4) and (5) are positive for $x_r > 0$, thus RH waves are amplified by protons (assuming $A_p < 0$) when $x_r < x_p^* = -A_p\,(A_p+1)^{-1}$ and are damped when $x_r > x_p^*$. The corresponding critical frequency, x_α^* that separates the range of dominant emission ($x_r < x_\alpha^*$) from that of prevailing absorption ($x_r > x_\alpha^*$), for αs

is $x^*_\alpha = -\frac{1}{2}\frac{A_\alpha}{A_\alpha+1}$. The approximate equations (4) and (5) are helpful to interpret the results of more precise numerical solutions of equation (3), and to understand trends in the changes of g under variations of the parameters.

2.2. Suprathermal Protons

[20] A power law in the tail of the distribution function of protons (f_p) have been observed (ISEE2 and ISEE3 data) in post-shock regions associated with solar ejecta material [*Gosling et al.*, 1981]. The presence of intermittent bidirectional fluxes of high energy protons along the magnetic lines (see, e.g., the review by *Gosling* [1990]) is a frequently observed feature during passages of ICMEs. To study the effects of energetic protons on the waves, we consider an additional component of non-Maxwellian protons. We derive now the dispersion relation for RH waves adding a minority group of protons with a decreasing power law in the parallel velocity. For the distribution f_m of the minority protons we assume a product of a κappa-function for $v_\parallel$ with a Maxwellian for $v_\perp$ as follows

$$f_m(v_\parallel, v_\perp) = n_m f_{\parallel,m}(v_\parallel) f_{\perp,m}(v_\perp), \tag{6}$$

with

$$f_{\parallel,m}(v_\parallel) = \frac{\Gamma(\kappa+1)}{\pi^{1/2}\theta_\parallel \kappa^{3/2}\Gamma(\kappa-1/2)}\left(1+\frac{v_\parallel^2}{\kappa\theta_\parallel^2}\right)^{-\kappa} \tag{7}$$

and

$$f_{\perp,m}(v_\perp) = \frac{1}{\pi\theta_\perp^2}\exp\left(-v_\perp^2/\theta_\perp^2\right) \tag{8}$$

where n_m is the density of the minority protons, and in equation (8) $\theta_\perp$ is the thermal velocity associated with $T_{\perp,m} = \frac{1}{2}m_p\theta_\perp^2$ where $T_{\perp,m}$ is the perpendicular temperature of the minority protons. In equation (7), Γ is the gamma function; κ is an integer, called the κ-index that defines the inverse power law; and $\theta_\parallel$ is a parameter that defines the spread of the κ distribution function. The relation between the second moment of f_m with respect to $v_\parallel$ and $\theta_\parallel$ is $T_{\parallel,m} = \frac{1}{2}m_p\theta_\parallel^2(1+\frac{3}{2\kappa-3}) > \frac{1}{2}m_p\theta_\parallel^2$ for $\kappa > 3/2$.

[21] Note that when the κ index tends to infinity, the κ function tends to a Maxwellian with $\theta_\parallel$ as its thermal velocity (i.e., $\lim_{\kappa\to\infty} T_{\parallel,m} = \frac{1}{2}m_p\theta_\parallel^2$). The κ-distribution has a shape similar to a Maxwellian for energies below the thermal energy, but exceeds the Maxwellian form at higher energies where the κappa distribution approximates a power law $f_\kappa \sim v_\parallel^{-2\kappa}$ [*Summers and Thorne*, 1991].

[22] Waves in space plasmas have been studied in several papers using κappa functions [e.g., *Summers and Thorne*, 1991, 1992; *Xue and Thorne*, 1993]. In most works the entire proton population has been represented by a κ function. However, in the context of ICME physics, we prefer to assume a κappa function only for a minority population of energetic protons, and only for their parallel velocity component in order to analyze the effect of energetic tails, keeping control on the relative abundance of protons that escape along the magnetic lines.

[23] For a plasma composed of a proton core population, αs, and electrons, all bi-Maxwellians, and a fraction of energetic protons with a distribution function defined by equation (6), the dispersion relation is obtained by adding the following term to the right hand of equation (3) (for a brief derivation see Appendix A),

$$\eta_m\Bigg[-1+\frac{\kappa-1/2}{\kappa-3/2}(A_\kappa+1)-\left(\frac{\kappa-1}{\kappa-3/2}\right)^{3/2}Z_{\kappa-1}\left(\sqrt{\frac{\kappa-1}{\kappa-3/2}}\frac{x+1}{y\beta_{\parallel,m}^{1/2}}\right)\Big/\left(y\beta_{\parallel,m}^{1/2}\right)+\left(\frac{\kappa}{\kappa-3/2}\right)^{3/2}(A_\kappa+1)\frac{x+1}{y\beta_{\parallel,m}^{1/2}}Z_\kappa\cdot\left(\sqrt{\frac{\kappa}{\kappa-3/2}}\frac{x+1}{y\beta_{\parallel,m}^{1/2}}\right)\Bigg]. \tag{9}$$

[24] Here $\eta_m = n_m/n_p$ (with n_p the density of the bi-Maxwellian protons) is the relative abundance of the minority protons; $A_\kappa = T_{\perp,m}/T_{\parallel,m} - 1$ is the thermal anisotropy of the κ-protons; $\beta_{\parallel,m} = 8\pi n_p T_{\parallel,m}/B^2 = \beta_p\,(T_\kappa/T_p)/(\frac{2}{3}A_\kappa + 1)$, where $T_\kappa = (2T_{\perp,m} + T_{\parallel,m})/3$; and Z_κ is the modified plasma dispersion function [*Summers and Thorne*, 1991]. Z_κ is a complex rational function and for $\kappa = 3$, the index used in this work (in agreement with *Gosling et al.* [1981]), the functions needed in equation (9) are $Z_3(\xi)$ and $Z_2(\xi)$, which are given by

$$Z_2(\xi) = -\frac{3\xi^2/4 + 9\sqrt{2}i\xi/4 - 4}{\left(\xi+\sqrt{2}i\right)^3}$$

$$Z_3(\xi) = -\frac{5\xi^3/6 + 10\sqrt{3}i\xi^2/3 - 29\xi/2 - 8\sqrt{3}i}{\left(\xi+\sqrt{3}i\right)^4}$$

[25] We consider parameter scenarios with η_m from 0% up to 15%, $T_\kappa/T_p = 2$, and $A_\kappa = A_p$.

[26] We solve exactly the dispersion relations of sections 2.1 and 2.2 using a numerical code to evaluate the plasma Zeta function, and standard optimization software to compute the roots of the complete dispersion relation. From these roots we obtain the complex dimensionless frequency $x = x_r + ig$, as a function of the wave number y, keeping constant the following input parameters: $\{\beta_p, A_p\}$; $\{\eta_m, A_\kappa, T_\kappa/T_p\}$; $\{\eta_\alpha, A_\alpha, T_\alpha/T_p\}$; $\{A_e, T_e/T_p\}$.

3. Numerical Results on the Excitation of the Waves

[27] For each chosen parameter scenario, we compute the dimensionless complex frequency $x = x_r + ig$ as a function of the normalized real wave number y, and we present figures in which the upper panel shows $g > 0$ (emission) vs x_r, the middle panel gives $-g > 0$ (absorption) vs x_r, and the bottom panel shows y vs x_r.

3.1. Influence of Proton Properties

[28] Here we study the effect of thermal and suprathermal properties of protons on the wave activity.

3.1.1. Thermal Properties

[29] We consider first variations of β_p. Figure 1 shows results for a case with a moderate negative thermal anisotropy of the protons, such as $A_p = -0.67$ (i.e., $T_{\parallel,p}/T_{\perp,p} = 3$)

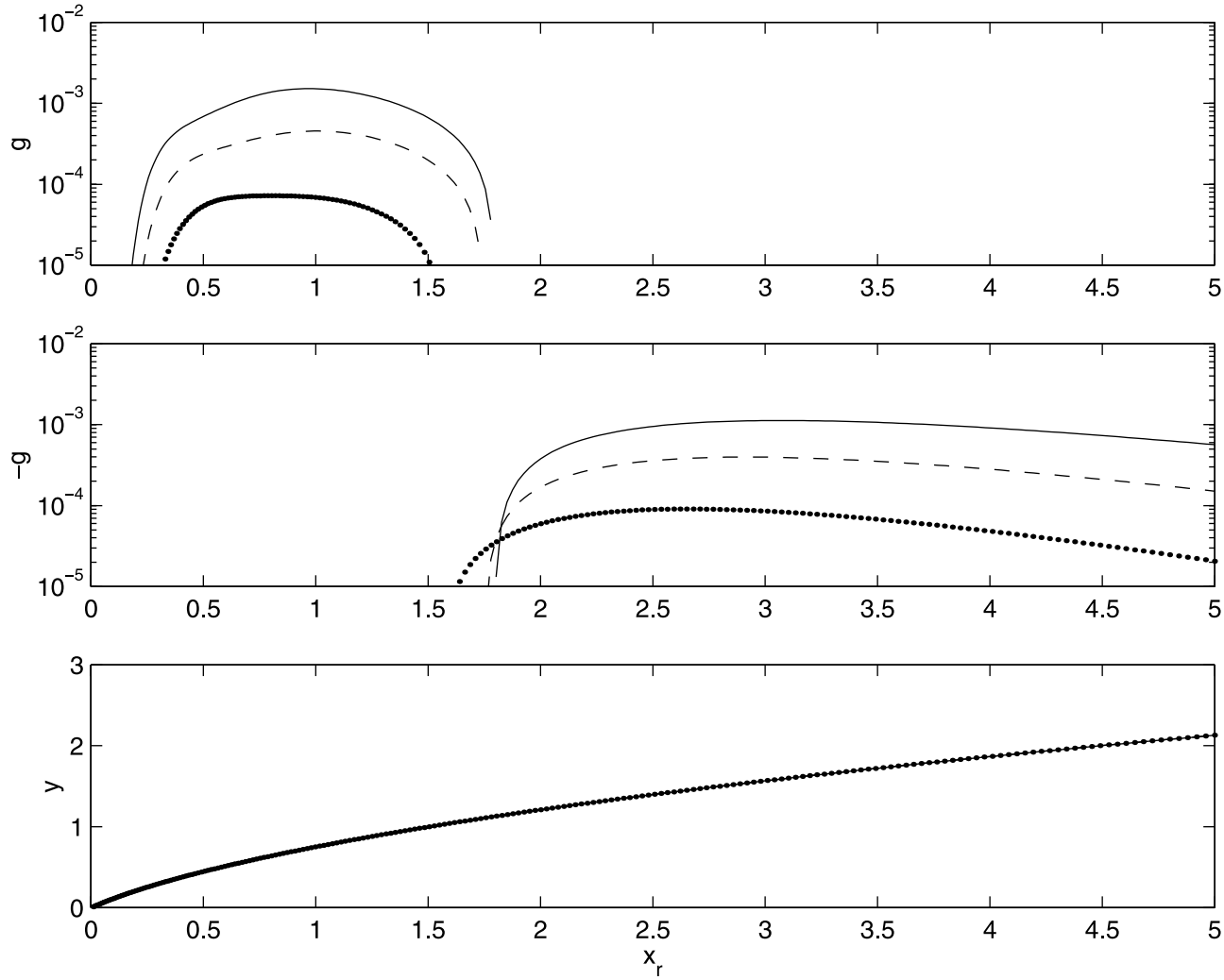

Figure 1. Dimensionless growth rate, g, damping rate, $-g$, and wave number, y, versus dimensionless frequency, x_r, for right-hand polarized EICWs (all rates and frequencies in units of the proton cyclotron frequency). The dot, dash, and solid lines correspond to the cases with $\beta_p = 0.4$, 0.5, and 0.6, respectively (with $A_p = -0.67$, $T_\alpha/T_p = 4$, $A_\alpha = -0.67$, $\eta_\alpha = 0.04$, and $A_e = 0$ constants).

with thermal velocity and thermal anisotropy of the alpha particles equal to that of the protons (i.e., $T_\alpha/T_p = 4$, $A_\alpha = -0.67$), low abundance of alpha particles $\eta_\alpha = 4\%$, and isotropic electrons, i.e., $A_e = 0$. When the electrons are isotropic, changes of T_e do not affect the EICWs instability [*Gratton et al.*, 1998]. The curves in Figure 1 are parameterized by β_p, and the values $\beta_p = 0.4$, 0.5, and 0.6 are represented by dotted, dashed, and continuous lines, respectively; the other quantities are fixed.

[30] From the upper panel of Figure 1 we can see that the maximum dimensionless growth rate g changes by a factor of about 20 as we raise beta from $\beta_p = 0.4$ to $\beta_p = 0.6$. We may note that for $\beta_p = 0.4$, the emission rates are larger than 10^{-5} in the frequency range $0.3\Omega_p < \omega < 1.5\ \Omega_p$, but are always smaller than 10^{-4}.

[31] To illustrate the meaning of these values, let us consider a magnetic field = 15 nT (i.e., $\Omega_p \sim 1$ rad/sec). Then $g = 10^{-5}$ gives an e-folding time $\tau = 1/\gamma$ of about 18 hours. Growth rates in this range are probably too slow to be physically significant. On one hand, the system always contains a level of field and particle fluctuations (not considered in our theory) that may scatter and damp extremely slow growing processes due to particle-wave resonance. On the other hand, it is not realistic to expect that the average background values, assumed constant by the wave theory, remain unchanged for very long periods of time because some evolve, for example, with distance from the Sun.

[32] The maximum growth rate is very sensitive to the value of β_p, with τ decreasing from 20 hours to 8 min (corresponding to $g = 1.5 \times 10^{-3}$) as β_p goes from 0.4 to 0.6. Note also that when $g = 1.5 \times 10^{-3}$, $\tau\Omega_p/2\pi = 146$, so that the wave amplitude increases by a factor 2.72 every 146 proton gyrations. Typical growth times of a few minutes correspond to significant excitation of the instability. Thus, values of g of $\sim 5 \times 10^{-4}$ ($\tau \sim 20$ minutes), or above, can be considered as physically interesting. Therefore, for ICMEs with parameters as considered in Figure 1, EICWs will be excited when $\beta_p \gtrsim 0.5$. However, as it will be shown in next sections, other observed ICMEs properties can favor the development of the instability, enabling significant growth rates to be reached with lower values of β_p.

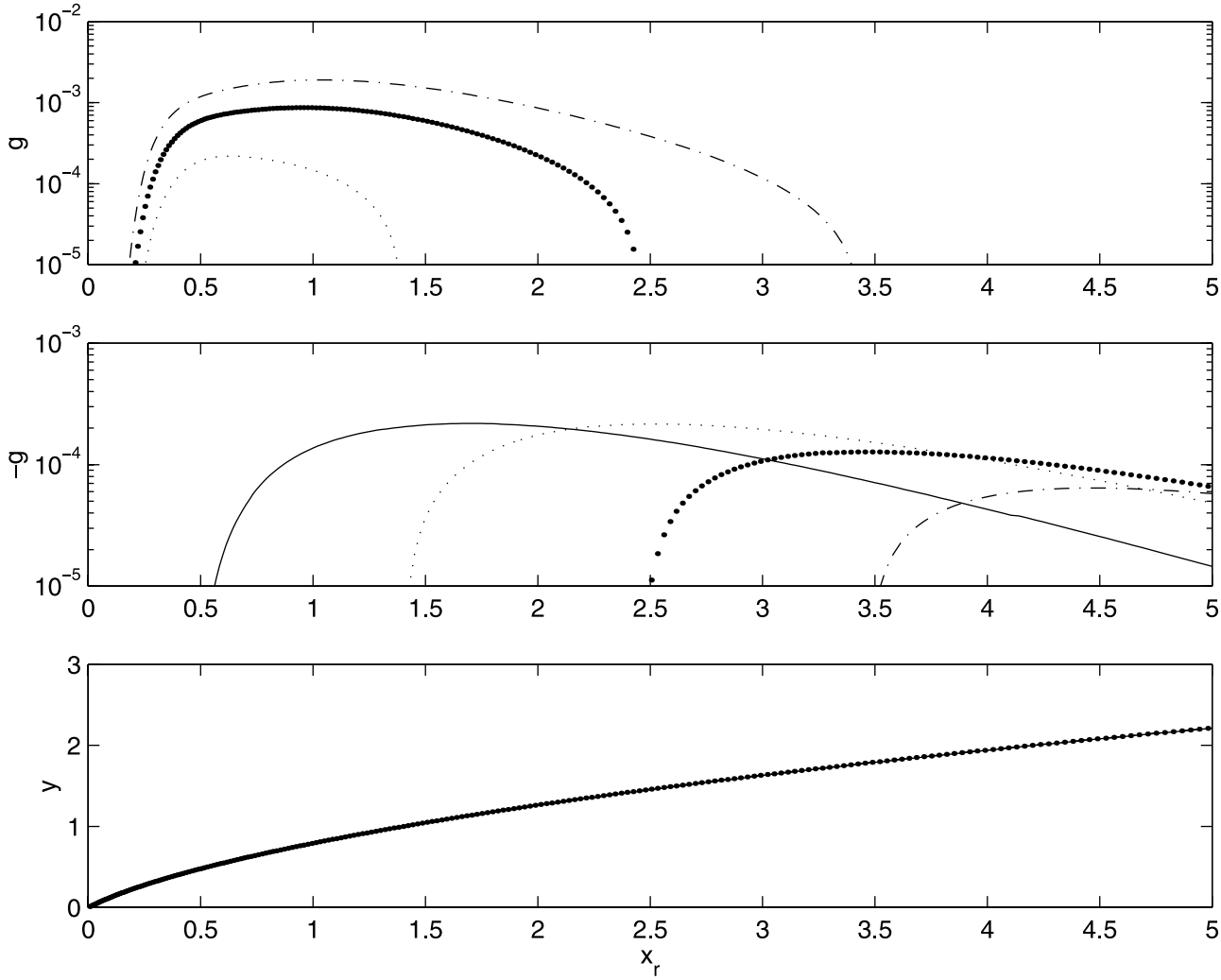

Figure 2a. Dimensionless growth rate, g, damping rate, $-g$, and wave number, y, versus dimensionless frequency, x_r, for right-hand polarized EICWs (all rates and frequencies in units of the proton cyclotron frequency). The solid, small-dot, big-dot, and dot-dash lines correspond to the cases with $A = A_p = A_\alpha = -0.5$, -0.67, -0.75, and -0.8, respectively (with $\beta_p = 0.4$, $T_\alpha/T_p = 4$, $\eta_\alpha = 0.08$, and $A_e = 0$ constants).

[33] From the middle panel of Figure 1, we may note that an absorption frequency range begins where the unstable range ends. The critical normalized frequency, x_r^*, where g changes sign, separates the frequencies $x_r < x_r^*$, for which there are more ions emitting than waves absorbing, from frequencies $x_r > x_r^*$, for which the reverse is true. We note also that, while the critical frequency for each ion species, depending on the A_s alone does not change with beta (see section 2.1), the combined effect of protons and αs determine a joint x_r^* that does vary with the beta parameter. In the majority of the examples studied here, as we move from lower to higher frequencies, we first find wave excitation with $g > 0$, followed by absorption $g < 0$ as we pass beyond x_r^*. After reaching a maximum damping rate, of the same order of magnitude as the preceding growth rates, $|g|$ decreases slowly as x_r continues to increase. In a few instances, to be examined later, the behavior for small values of x_r is different.

[34] From the dimensionless wave number, y, shown in the bottom panel of Figure 1 as a function of x_r, we may note that no change in the phase velocity of the waves can be perceived as β_p varies from 0.4 to 0.6.

[35] In Figures 2a and 2b we examine the effect of changes in the thermal anisotropy of the ions. Here A_p is varied from -0.5 to -0.8 (i.e., $T_\parallel/T_\perp$ from 2 to 5). As discussed in section 3.3 we set $A_\alpha = A_p$, so that the anisotropy of αs also changes. We keep $\beta_p = 0.4$ constant, at the lowest level considered in Figure 1, and $T_\alpha/T_p = 4$, $\eta_\alpha = 8\%$, and $A_e = 0$ are also fixed parameters, where the α abundance is twice as large as in the previous example. Again, for the variations of A_p considered here no significant change of the wave velocity can be observed. As can be seen in the top panel, increasing $|A|$ has a substantial effect on the growth rates: not only g rises by two orders of magnitude as A changes from -0.5 to -0.8, but also the unstable frequency range increases by a factor of $\sim$2. The lower frequency of the unstable range, where $g = 10^{-5}$, shifts slowly toward smaller frequencies. Maximum growth rates for a ICME with $B \sim 15$ nT, correspond to instability e-folding times of 6 minutes, 14 minutes, 54 minutes, and 46 hours (the rate for the last time is $g < 10^{-5}$ [not shown in

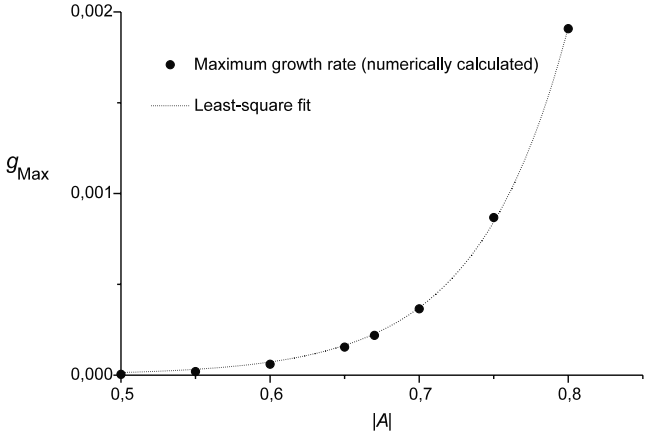

Figure 2b. The maximum growth rate increases exponentially with $|A|$. g_{Max} ($|A|$) = a exp($b|A|$). With a least-squares fit we obtained the following values corresponding to the cases of Figure 2a, $a = 3.9 \times 10^{-9}$ and $b = 16.4$.

Figure 2a]) for $A = -0.8, -0.75, -0.67, -0.5$, respectively. The middle panel of this figure shows that, as in cases shown in Figure 1, the absorption band extends prominently beyond frequencies $\sim 5\Omega_p$, where $g > 10^{-5}$ for the four studied cases.

[36] We find further that the maximum growth rate increases exponentially with $|A|$, i.e., g_{Max} ($|A|$) = a exp($b|A|$) (Figure 2b). Using the rest of the parameters as in Figure 2a and doing a least-squares fit, we obtained the following values: $a = 3.9 \times 10^{-9}$ and $b = 16.4$.

[37] Runs with $A_p = -0.8, -0.75, -0.67, -0.5$, but with $A_\alpha = -0.67$ fixed and all other parameters same as in Figure 2a were also made (not shown). The results show basically similar behavior except for the growth rate curve for the lowest $|A_p|$, ($A_p = -0.5$), where g now reaches a maximum value of $>10^{-4}$ and the unstable range extends from 0.2 to 1. Furthermore, the frequency where g change its sign (i.e., x_r^*) now practically does not change with different values of A_p. Variations on both, $A = A_p = A_\alpha$, and only A_p (keeping A_α fixed), have no significant effect on the wave speed.

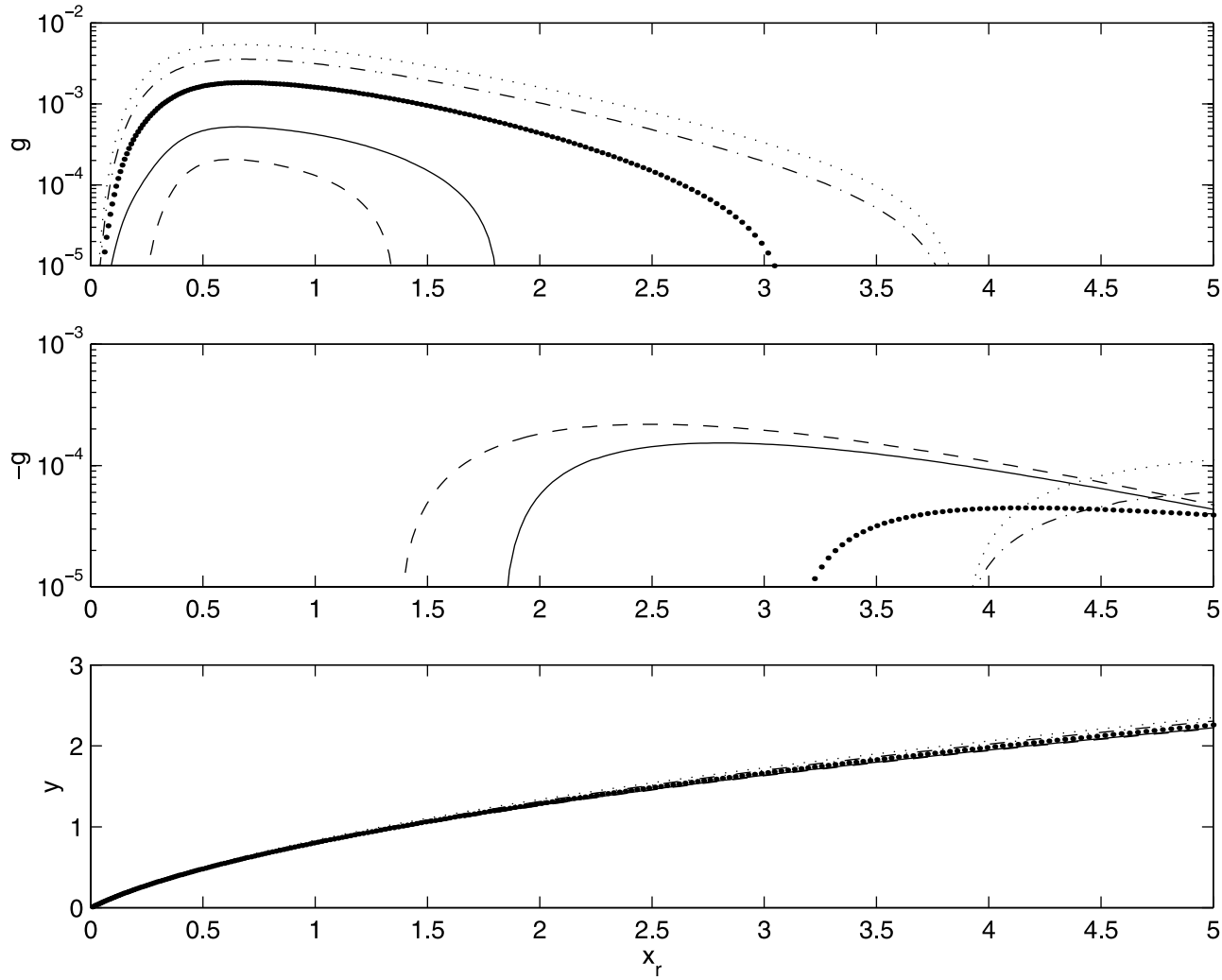

Figure 3a. Dimensionless growth rate, g, damping rate, $-g$, and wave number, y, versus dimensionless frequency, x_r, for right-hand polarized EICWs (all rates and frequencies in units of the proton cyclotron frequency). The dash, solid, big-dot, dot-dash, and small-dot lines correspond to the cases with $\eta_\kappa = 0$, 0.01, 0.05, 0.1, and 0.15, respectively (with $\beta_p = 0.4$, $A_p = A_\alpha = A_\kappa = -0.67$, $T_\kappa/T_p = 2$, $T_\alpha/T_p = 4$, $\eta_\alpha = 0.08$, and $A_e = 0$ constants).

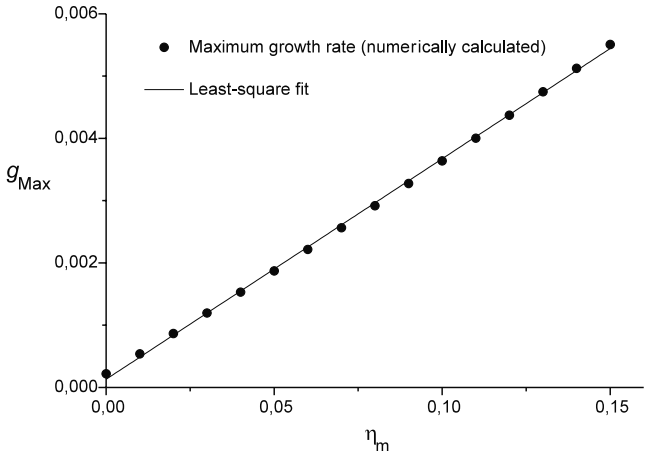

Figure 3b. The maximum growth rate depends linearly on η_m. $g_{Max}(\eta_m) = a_1\eta_m + b_1$. With a least-squares fit we obtained the following values corresponding to the cases of Figure 3a, $a_1 = 0.0354$ and $b_1 = 0.0001$.

3.1.2. Suprathermal Properties

[38] We analyze now the effects on the waves of suprathermal wings along B_0, considering an additional component of non-Maxwellian protons as was explained in section 2.2. Figure 3 shows results for cases with $\beta_p = 0.4$, $A_\alpha = A_p = A_\kappa = -0.67$, $T_\alpha/T_p = 4$, $\eta_\alpha = 0.08$, isotropic electrons (i.e., $A_e = 0$), $T_\kappa = 2T_p$, $\kappa = 3$, all of them fixed. The five curves of the Figure 3a correspond to different abundance of suprathermal protons (the relative abundance of minority protons respect to the core proton density) from 0 to 15%. The dashed, solid, big-dotted, dot-dashed, and small-dotted lines correspond to the cases with $\eta_m = 0$, 0.01, 0.05, 0.1, and 0.15, respectively. The growth rates and the widths of the unstable frequency bands increase as η_m increases, e.g., the maximum g for $\eta_m = 5\%$ is 3 times the g value for $\eta_m = 1\%$, and the width of the unstable frequency range approximately doubles. Note that when η_m goes from 0 to 15%, g_{Max} goes from $\sim 2 \times 10^{-4}$ to $\sim 5 \times 10^{-3}$, a 25-fold increase, which is a large effect. The bottom panel shows that again that the wave speed is almost unaffected by variation of η_m and thus the intensi-

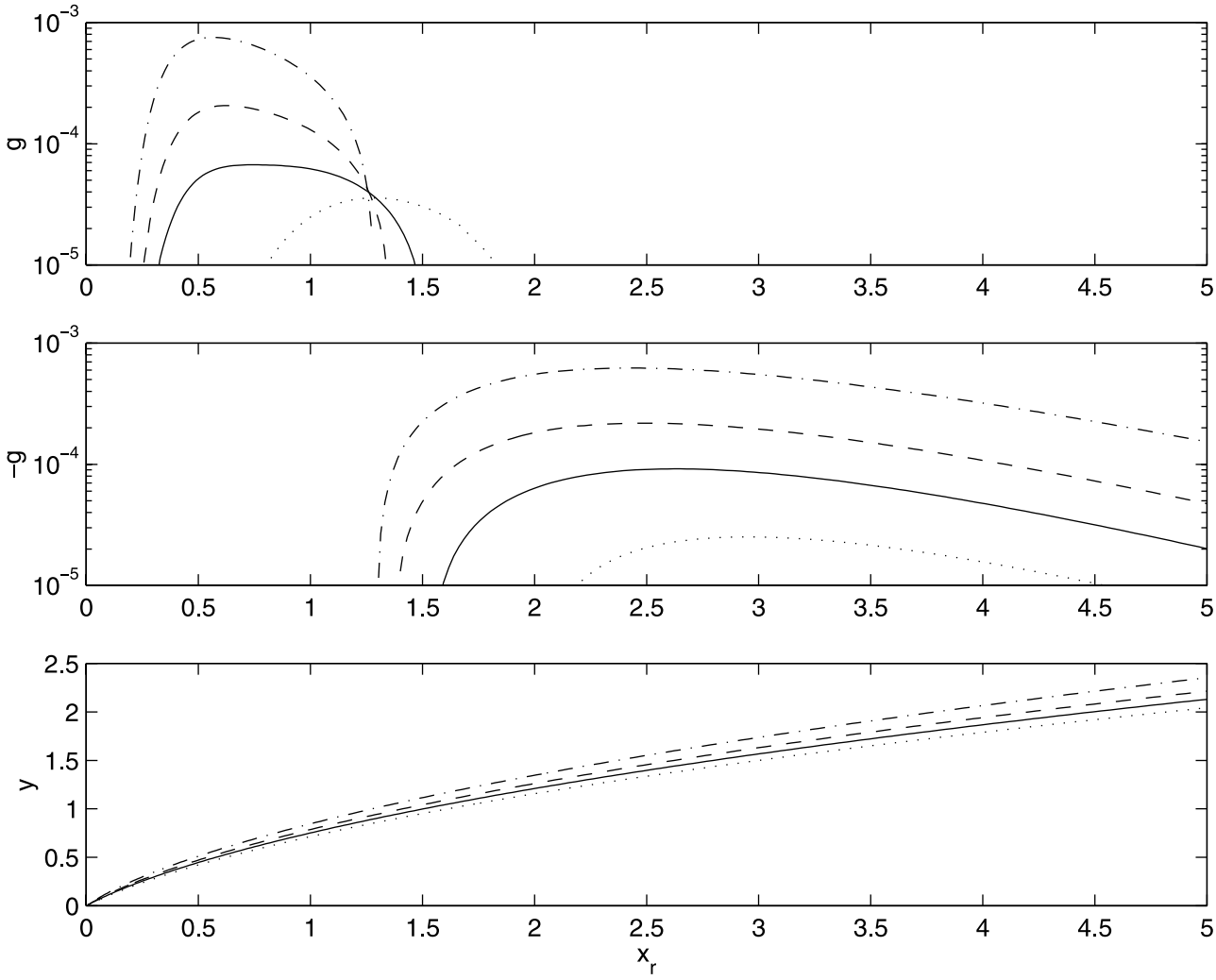

Figure 4. Dimensionless growth rate, g, damping rate, $-g$, and wave number, y, versus dimensionless frequency, x_r, for right-hand polarized EICWs (all rates and frequencies in units of the proton cyclotron frequency). The dot, solid, dash, and dot-dash lines correspond to the cases with $\eta_\alpha = 0$, 0.04, 0.08, and 0.15, respectively (with $\beta_p = 0.4$, $A_p = A_\alpha = -0.67$, $T_\alpha/T_p = 4$, and $A_e = 0$ constants).

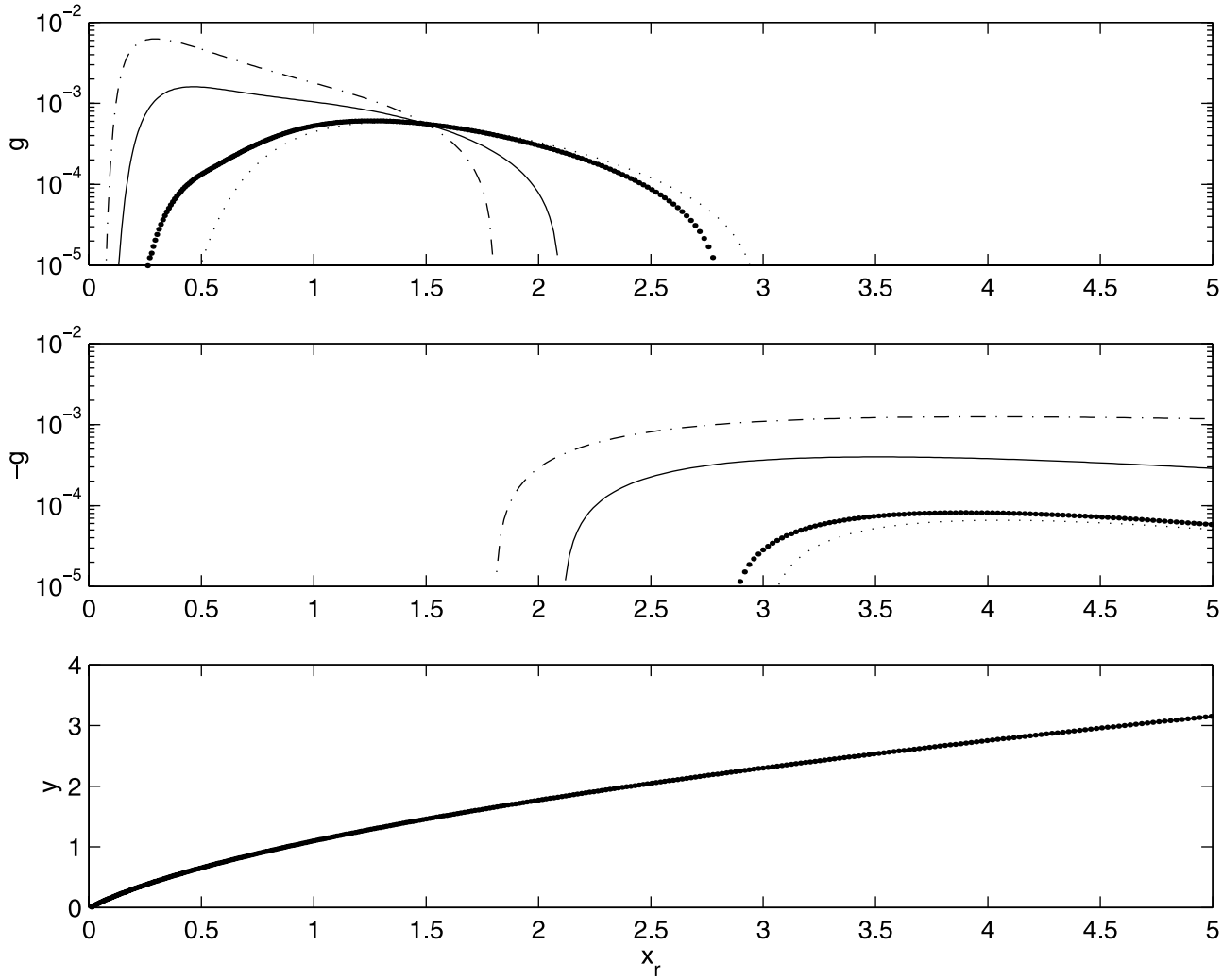

Figure 5. Dimensionless growth rate, g, damping rate, $-g$, and wave number, y, versus dimensionless frequency, x_r, for right-hand polarized EICWs (all rates and frequencies in units of the proton cyclotron frequency). The small-dot, big-dot, solid, and dot-dash lines correspond to the cases with T_α/T_p = 1, 4, 8, and 16, respectively (with β_p = 0.2, $A_p = A_\alpha = -0.75$, η_α = 0.02, T_e/T_p = 7, $A_e = -0.5$ constants).

fication of the instability is only a consequence of add a few protons in the resonant region of the tail of the proton distribution function.

[39] Further analysis (Figure 3b) shows that g_{Max} increases linearly with η_κ as $g_{Max} = a_1\eta_\kappa + b_1$, where for the chosen parameters, $a_1 = 3.5 \times 10^{-2}$ and $b_1 = 1.3 \times 10^{-4}$. It is possible to fit [not shown] the relationship between the width of the unstable frequency band (Δx_r) and η_m by $\Delta x_r = a_2 - b_2 \exp(-c_2\eta_\kappa^{d_2}$ where a_2 = 4.01, b_2 = 2.76, c_2 = 45.40, and d_2 = 1.22 for the set of parameters chosen in Figure 3a. The width of the unstable frequency range saturates near η_m = 10%.

3.2. Influence of Alpha Particles

[40] In this section we analyze the effects of properties of αs on the instability. We find that even when the abundance of αs relative to protons is as low as 2%, αs can be crucial for determining the level of the instability of EICWs. The results of the influence of alpha particle on the growth and absorption rates of the EICW instability are presented in Figures 4–6.

[41] Figure 4 shows configurations with different alpha particle abundances ($\eta_\alpha = n_\alpha/n_p$ = 0, 0.04, 0.08, and 0.15) and β_p = 0.4, $A_p = A_\alpha = -0.67$, T_α/T_p = 4, and A_e = 0, maintained constants. An increment of η_α produces a growth of the instability rates and shifts the active range to lower frequencies. When η_α = 0.15, the maximum value of the growth rate is $\gamma/\Omega_p = 8 \times 10^{-4}$ which occurs for ω_r/Ω_p = 0.56. In accordance with the increment of the growth rates, the damping rates also increase. Due to the increment of the inertia of the wave, its speed slows down when alpha particles are added to the plasma. Thus, the addition of αs has two effects: (1) modifications of the wave speed, allowing more ions (both protons and alphas) to be in resonant conditions; and (2) an increase of the number of resonant αs.

[42] We include the contribution of anisotropic electrons in cases shown in Figure 5 and Figure 6. Figure 5 illustrates the case where T_α/T_p changes from 1 to 16. The rest of the parameters are fixed: β_p = 0.2, $A_p = A_\alpha = -0.75$, η_α = 0.02 (a low alpha particle abundance), $A_e = -1/2$, and T_e/T_p = 7. The properties of the αs are chosen here according to the

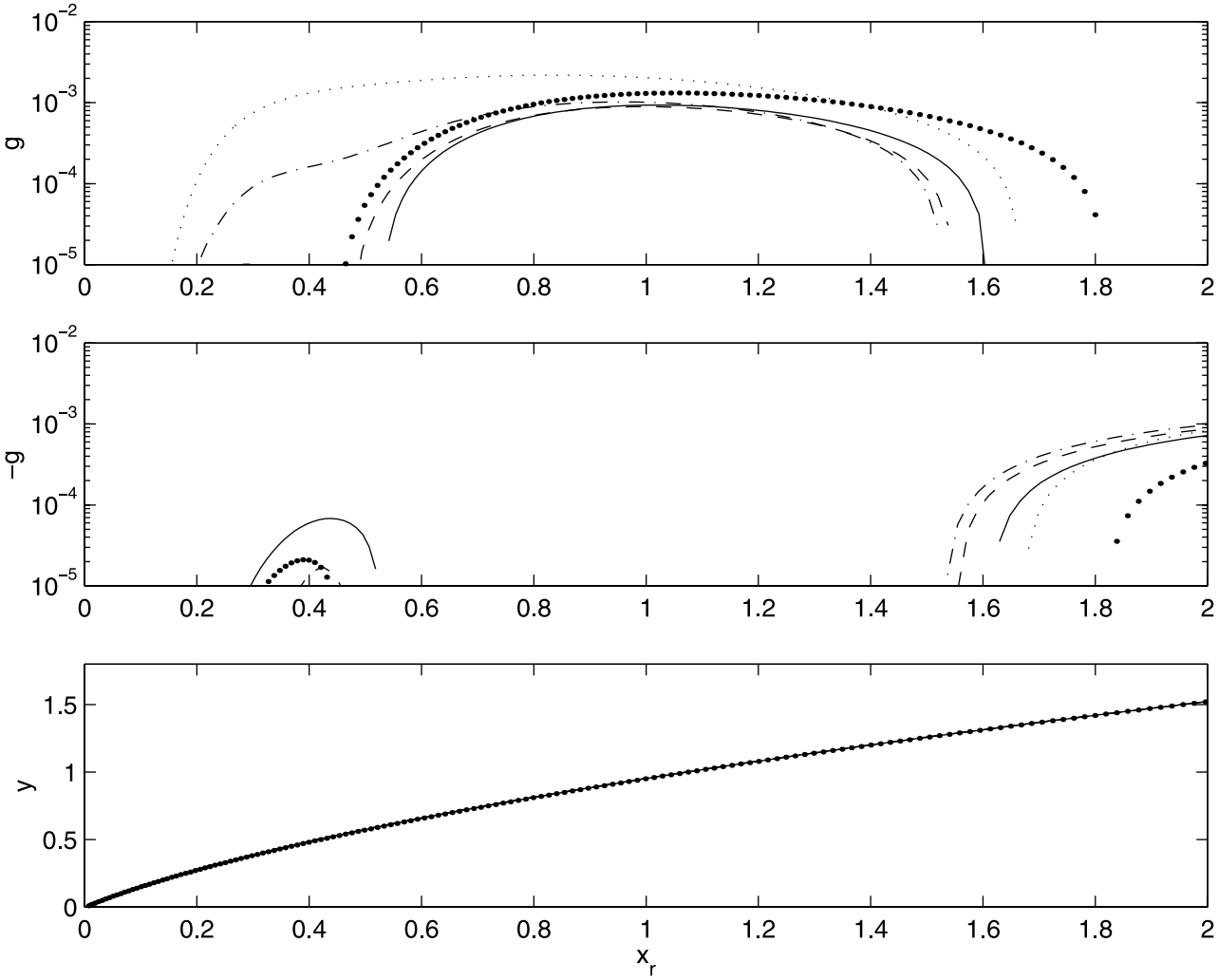

Figure 6. Dimensionless growth rate, g, damping rate, $-g$, and wave number, y, versus dimensionless frequency, x_r, for right-hand polarized EICWs (all rates and frequencies in units of the proton cyclotron frequency). The big-dot, solid, dash, dot-dash, and small-dot lines correspond to the cases with $A_\alpha = 0$, -0.3, -0.4, -0.5, -0.67, respectively (with $\beta_p = 0.4$, $A_p = -0.67$, $\eta_\alpha = 0.08$, $T_\alpha/T_p = 4$, $T_e/T_p = 7$, $A_e = -0.17$ constants).

values of the thermal velocity and abundance reported by [*Burlaga et al.*, 1998]. The upper panel of Figure 5 shows a strong increment of the growth rates as T_α/T_p increases. The maximum rate increases almost one order of magnitude (from $g_{Max} \sim 10^{-3}$ to $g_{Max} \sim 10^{-2}$) when T_α/T_p varies between 4 and 16. Moreover, the frequency at which the growth rate maximizes shifts to substantially lower values when T_α/T_p increases. While for $T_\alpha/T_p = 4$ the frequency that corresponds to g_{Max} is $\omega_r \sim 1.5\Omega_p$, when $T_\alpha/T_p = 16$ it is $\omega_r \sim 0.25\Omega_p$. The phase speed of the wave does not change substantially when T_α/T_p varies. Cases with $T_\alpha/T_p = 1$ and $T_\alpha/T_p = 4$ have very similar growth rates, except for the lower frequencies $\omega_r \epsilon (\frac{1}{4}\Omega_p, \frac{1}{2}\Omega_p)$. In this frequency range, the waves are practically stable for $T_\alpha/T_p = 1$, but they are unstable for $T_\alpha/T_p = 4$. For $\omega_r \epsilon (2.8\Omega_p, 3\Omega_p)$, when $T_\alpha/T_p = 1$, the waves are amplified, but when $T_\alpha/T_p = 4$ they are absorbed. These results can be compared with a new scenario, where all the alpha particles are removed ($\eta_\alpha = 0$). Here, we find that the new maximum growth rate reaches just $g_{Max} \sim 3 \times 10^{-4}$ (not shown), a value which is lower than the case with $\eta_\alpha = 0.02$ and $T_\alpha/T_p = 1-4$. The ICME scenario studied in Figure 5 contains a very low alpha particle abundance, even lower than the typical abundance observed in the solar wind. Thus, in ICMEs with similar properties, but having a higher alpha abundance, the growth and absorption rates will be increased with respect to the results of Figure 5, according to Figure 4.

[43] Different curves in Figure 6 illustrate cases where $A_\alpha \neq A_p$. In particular, different examples with values of A_α from 0 to -0.67, keeping $A_p = -0.67$ constant, are shown in this figure. The rest of the parameters are fixed at $\beta_p = 0.4$, $T_\alpha/T_p = 4$, $\eta_\alpha = 0.08$, $A_e = -0.17$ ($T_{\parallel,e}/T_{\perp e} = 1.2$), and $T_e/T_p = 7$.

[44] The small-dotted line in Figure 6 represents the case with $A_\alpha = A_p = -0.67$, it shows a single and wide unstable band between $0.16\Omega_p$ and $1.7\Omega_p$. When A_α is increased (i.e., the anisotropy is lowered), a plateau is formed for $A_\alpha \sim -0.5$ (dash-dotted line) in the growth rate curve (upper panel) around $\omega_r \sim 0.4\Omega_p$. When A_α increases further, e.g., cases with $A_\alpha \sim -0.4$ (dashed line), the unstable band tends to be

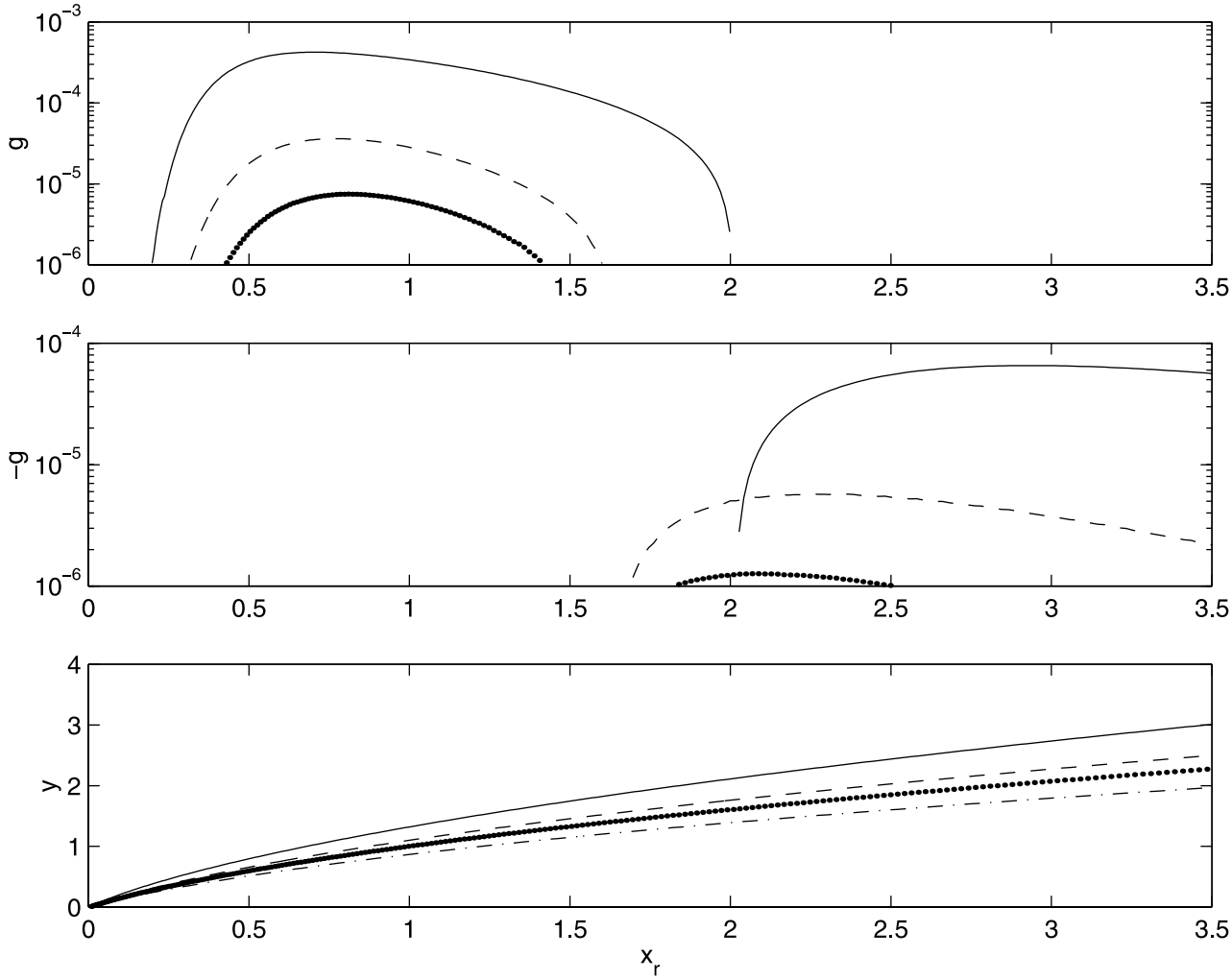

Figure 7a. Dimensionless growth rate, g, damping rate, $-g$, and wave number, y, versus dimensionless frequency, x_r, for right-hand polarized EICWs (all rates and frequencies in units of the proton cyclotron frequency). The dash-dot, dot, dash, and solid lines correspond to the cases with T_e/T_p = 1, 5, 7, and 10, respectively (with $\beta_p = 0.12$, $A_p = -0.75$, $T_\alpha/T_p = 4$, $A_\alpha = -0.75$, $\eta_\alpha = 0.15$, $A_e = -0.5$ constants).

narrow, and two absorption bands appear (see cases $A_\alpha = -0.4$, $A_\alpha = -0.3$, and $A_\alpha = 0$ in the middle panel). For the case containing isotropic αs ($A_\alpha = 0$, shown as a big-dotted curve) a weak absorption band starts at $\omega \sim 0.25\Omega_p$ and ends at $\omega \sim 0.44\Omega_p$, followed by an unstable band that goes up to $\omega \sim 1.83\Omega_p$. Finally, a second larger absorption band extends to frequencies larger than $2\Omega_p$.

[45] From a theoretical point of view, as discussed in section 2.1, cases with double absorption bands appear only when the frequency ω_p^*, where g_p changes its sign, is different from ω_α^*. For protons with $A_p = -0.67$, $\omega_p^*/\Omega_p = -A_p/(A_p + 1) = 2$, and for alpha particles with $A_\alpha = -0.3$, $\omega_\alpha^*/\Omega_p = -\frac{1}{2}A_\alpha(A_\alpha + 1)^{-1} = 0.21$. Thus, in the case shown as a solid line in Figure 6, the protons emit waves for $\omega_r < 2\Omega_p$ and damp them for $\omega_r > 2\Omega_p$. On the other hand, the waves are excited by αs for $\omega_r < 0.21\Omega_p$, and they are damped when $\omega_r > 0.21\Omega_p$. Therefore, for frequencies lower than $0.21\Omega_p$ there is a marginally unstable band (not shown because $g \lesssim 10^{-5}$) as a consequence of a weak emission of waves from both ionic species. For frequencies between $0.21\Omega_p$ and $2\Omega_p$ protons emit waves but αs absorb them. In the frequency range from $0.21\Omega_p$ to $\sim 0.53\Omega_p$, αs absorb more waves than can protons emit and as a consequence an absorption band appears here (see solid line in the middle panel of Figure 6). However, for ω_r between $0.53\Omega_p$ and $1.61\Omega_p$, the opposite happens and an unstable band appears. Finally, a second damping band goes from $\sim 1.61\Omega_p$ to beyond $2\Omega_p$, reaching frequencies larger than $5\Omega_p$.

3.3. Influence of Electrons

[46] We analyze here the indirect effect of electrons on the waves activity. The thermal speed of thermal electrons is not enough to satisfy the resonant condition and, thus, they can only influence the instability by modifying the resonance conditions of the ions, i.e., lowering the phase velocity of the wave.

[47] For this study we take as a reference set the values $A_p = -0.75$ (corresponding to $T_{p,\parallel}/T_{p,\perp} = 4$), $\beta_p = 0.12$, $A_\alpha = -0.75$ ($=A_p$), $T_\alpha/T_p = 4$, $\eta_\alpha = 0.15$, $T_e/T_p = 10$, and $A_e = -0.5$ (corresponding to $T_{e,\parallel}/T_{e,\perp} = 2$). Note that in plasmas with very low β_p, as in our reference set, the development of this instability is in general not expected. However, we will

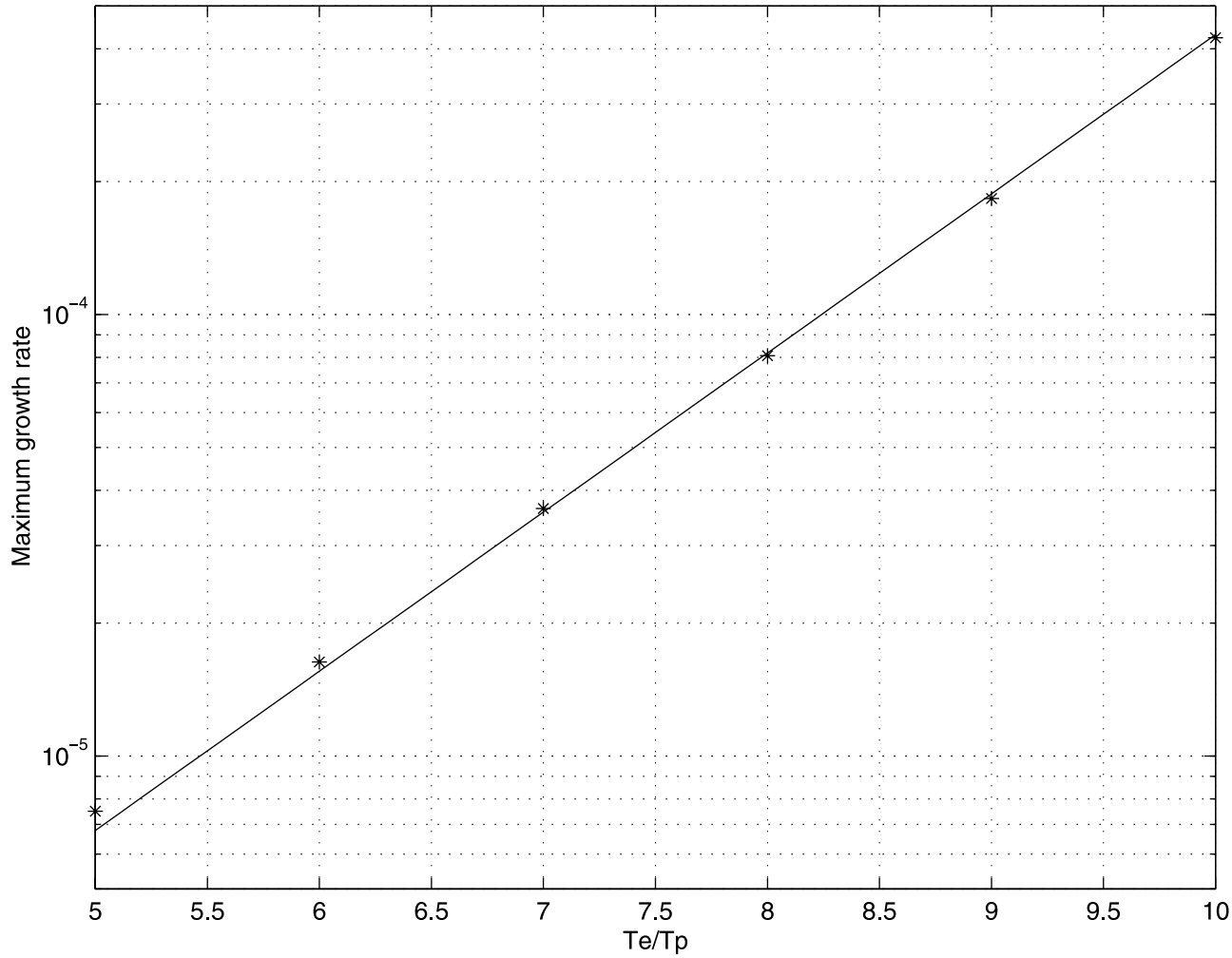

Figure 7b. Maximum dimensionless growth rate, g_{Max}, versus T_e/T_p for right-hand polarized EICWs. g_{Max} increases exponentially with T_e/T_p like $g_{Max} = A \exp(BT_e/T_p)$, with $A = 1.07 \times 10^{-7}$, and $B = 0.83$, obtained with a least-squares fit from Figure 7a. The solid line corresponds to the fitting, and the stars are growth rate values obtained numerically.

show possible ICME scenarios in which the instability is present even for values of β_p as low as $\sim$0.1.

[48] To bring out the effect of T_e/T_p, in Figure 7a we compare the reference case with results obtained for T_e/T_p = 1, 5, 7, respectively. The bottom panel shows that T_e/T_p has a considerable influence on the wave speed when A_e is negative: when T_e/T_p increases, the phase velocity decreases (see lower panel) allowing more ions to travel with the wave and resonate. Increasing T_e/T_p has a substantial effect on the growth rates. Thus, the maximum growth rate, g_{Max}, rises by almost two orders of magnitude as T_e/T_p goes from 5 to 10. The unstable frequency range is thereby also increased when the electron temperature reaches higher values. In the middle panel we can see that when T_e/T_p = 10, the absorption range, which starts when the unstable band ends close to $2\Omega_p$, reaches frequencies beyond $\omega_r = 5\Omega_p$. Furthermore, the critical frequency when g changes its sign shifts slowly toward higher frequencies when the electron temperature increases. Note that for T_e/T_p = 1 the EICWs are stable and, therefore, this condition is represented by the absence of dash-dotted lines in the upper and middle panels.

[49] Figure 7b illustrates the behavior of the maximum growth rate as T_e/T_p increases, for the same values considered in Figure 7a. We find that the maximum growth rate increases exponentially with T_e/T_p in the interval 5 to 10. Using a least-squares fit, we obtain $g_{Max} = A \exp(BT_e/T_p)$ with $A = 1.07 \times 10^{-7}$ and $B = 0.83$.

[50] We now consider the effect of A_e. Figure 8a shows results for $A_p = -0.75$, $\beta_p = 0.12$, $A_\alpha = -0.75 (= A_p)$, $T_\alpha/T_p = 4$, $\eta_\alpha = 0.15$, $T_e/T_p = 10$. We compute solutions of the dispersion relation for $A_e = 0, -0.3, -0.5, -0.55$, represented by dash-dotted, dashed, dotted, and solid lines, respectively. The bottom panel shows that the wave velocity is strongly influenced by A_e. In fact, the phase velocity is strongly affected by a combination of high T_e and $T_{\|,e} > T_{\perp e}$.

[51] The maximum growth rate when $A_e = -0.5$ is $g_{Max} = 4.2 \times 10^{-4}$, i.e., $\sim$56 times higher than the maximum growth rate corresponding to $A_e = -0.3$ ($g_{Max} = 7.5 \times 10^{-6}$). The case $A_e = 0$ is stable, so that dash-dotted lines do not appear in the panels for g and $-g$. A further examination shows that the maximum growth rate increases more steeply than exponential with $|A_e|$. Figure 8b shows a semilogarithmic plot of g_{Max} versus $|A_e|$. Assuming that g_{Max} =

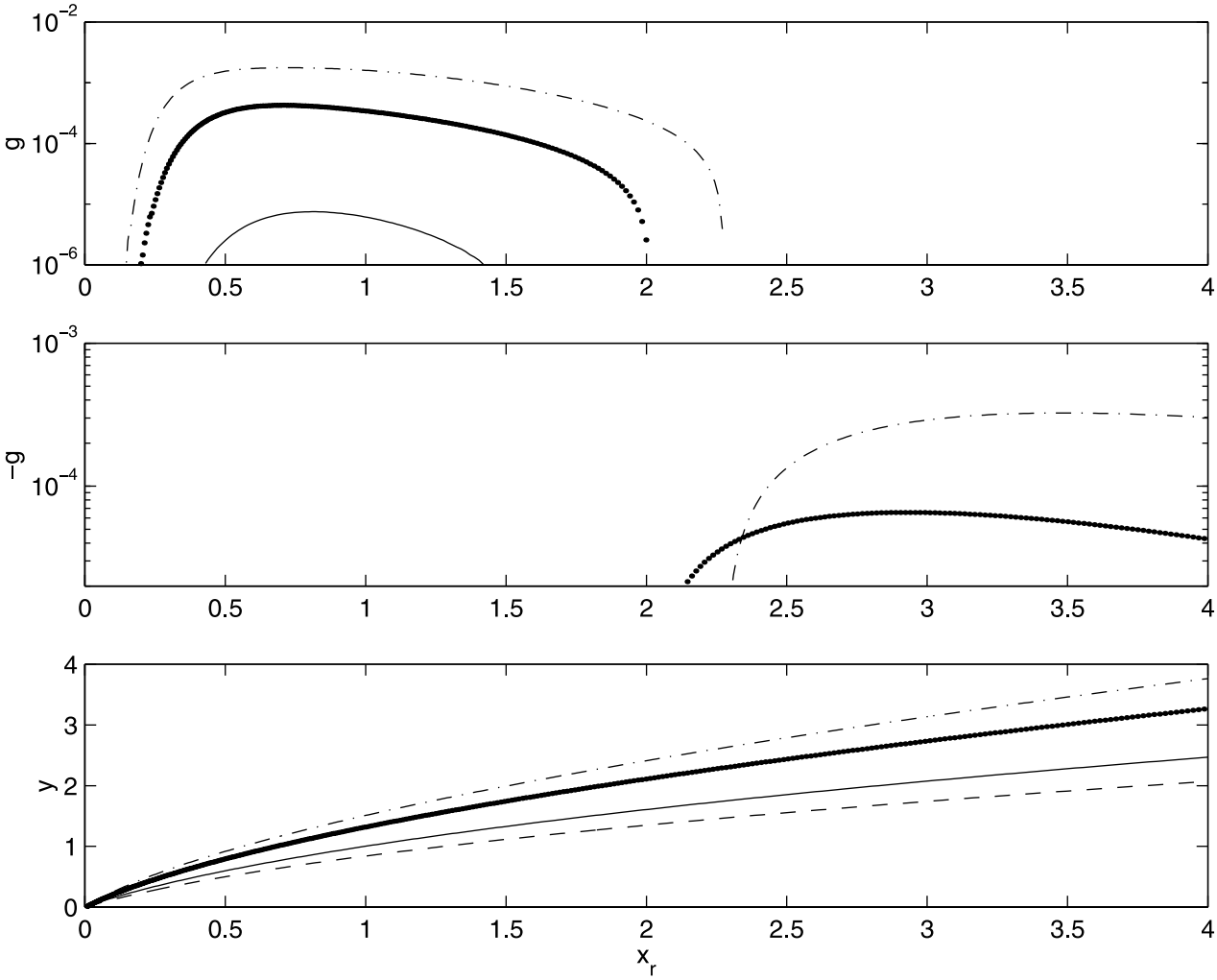

Figure 8a. Dimensionless growth rate, g, damping rate, $-g$, and wave number, y, versus dimensionless frequency, x_r, for right-hand polarized EICWs (all rates and frequencies in units of the proton cyclotron frequency). The dash, solid, dot, and dash-dot lines correspond to the cases with $A_e = 0$, -0.3, -0.5, and -0.55, respectively (with $\beta_p = 0.12$, $A_p = -0.75$, $T_\alpha/T_p = 4$, $A_\alpha = -0.75$, $\eta_\alpha = 0.15$, $T_e/T_p = 10$ constants).

$C\exp(D|A_e|\gamma)$ with $\gamma = 2$, and using a least-squares fit, we obtain $C = 4.7 \times 10^{-7}$ and $D = 28.3$ for the same values studied in Figure 8a.

4. Discussion and Conclusions

[52] This study has explored the influence of the properties of thermal ions (protons and alpha particles), thermal electrons, and suprathermal protons on the excitation of right-hand polarized EICWs in ICMEs. We have defined different parameter regimes consistent with the observed properties of solar ejecta and we have analyzed the trend of each parameter on the instability. In a variety of scenarios, significant EICW growth rates were possible, which lead us to believe that this kind of wave emission may be significant in ICMEs. In view of the fact that ICMEs form a heterogeneous group of objects, it is possible that right combinations of these properties occur only in some ICMEs, or even in isolated regions of the same ICME. Thus, even with respect to EICW activity, ICMEs form a heterogeneous collection with a wide range of activity levels (amplifying and damping) ranging from the insignificant to the pronounced.

[53] The presence of a negative thermal anisotropy (i.e., $T_\parallel > T_\perp$) favors the development of the instability; however, the physical mechanism involved is very different according to whether $T_\parallel > T_\perp$ applies to ions or to electrons. In the first case (ions), an enhancement of wave activity is brought about by the fact that more ions are moving near the resonant frequency. This is therefore a direct effect. In the second case (electrons), the enhanced wave activity is achieved through a slowing down of the waves by the fluid firehose effect, allowing more ions to resonate with the wave. This we call an indirect effect. Furthermore, the effects produced by variation of some ICME parameters imply the presence of the combined effects, i.e., they increase the number of resonant ions and also modify the wave velocity. Specifically, β_p, A_p, T_α/T_p, and A_α, have a direct effect, the thermal electrons (i.e., A_e and T_e/T_p) have a purely indirect effect, and, finally, the abundance of the minority suprathermal protons (η_m) and the

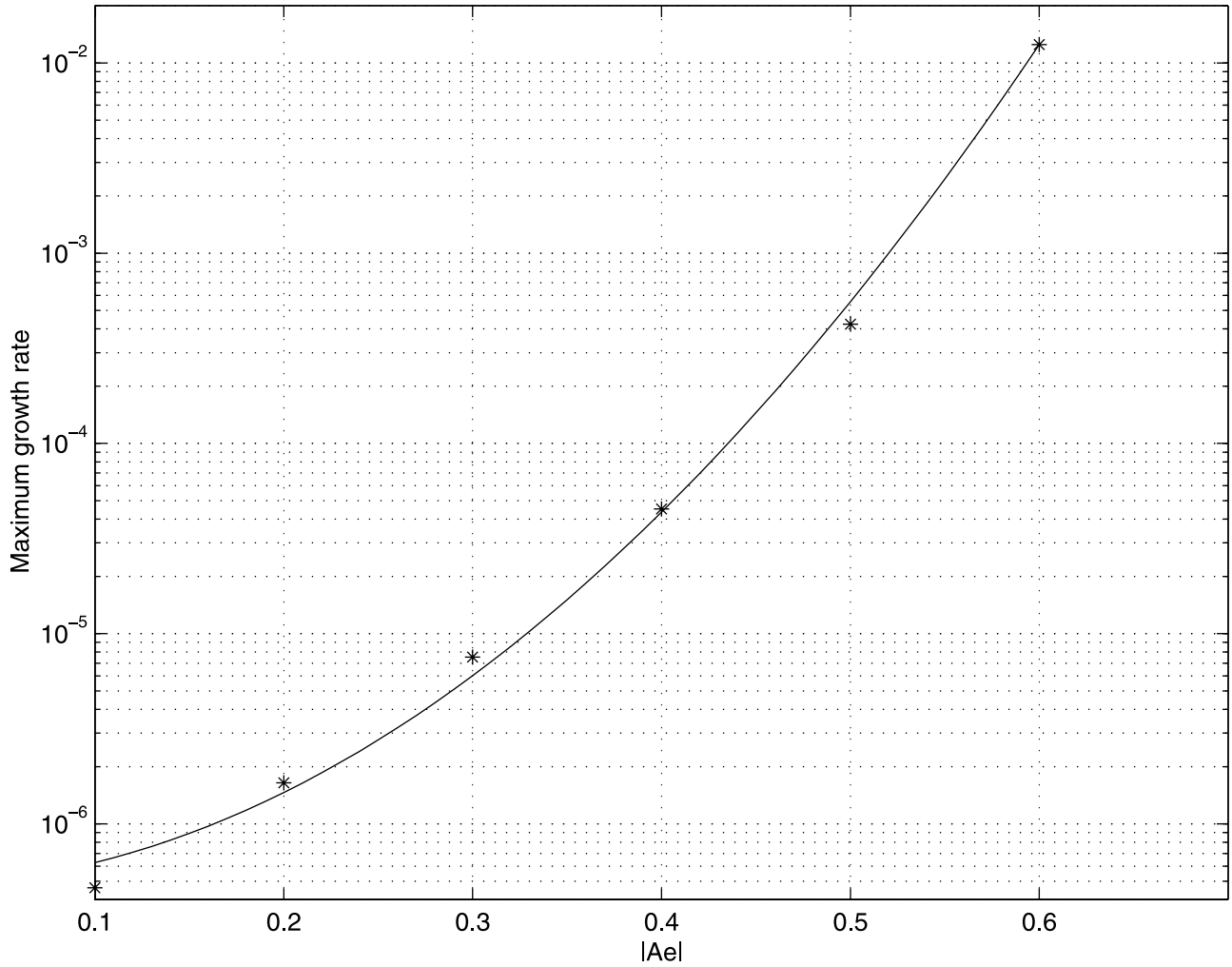

Figure 8b. Maximum dimensionless growth rate, g_{Max}, versus $|A_e|$ for right-hand polarized EICWs. g_{Max} increases more than exponentially with $|A_e|$. Assuming $g_{Max} = C\exp(D\ |A_e|^2)$, a least-squares fit gives, $C = 4.7 \times 10^{-7}$ and $D = 28.3$, for the same cases of Figure 8a. The solid line corresponds to the fitted curve, and the stars to roots computed numerically.

abundance of alpha particles (η_α) have a combined effect (direct and indirect).

[54] Among the set of parameters that enter in the dispersion relation, the proton plasma beta and the proton thermal anisotropy are very often the most relevant properties that decide whether the instability may be excited or not. However, we have shown that electrons can efficiently contribute to EICW emission and absorption. In particular, we have shown possible ICME scenarios with very low beta proton values ($\beta_p \sim 0.1$), where the instability develops with significant growth rates which translate to e-folding time of a few minutes when the rest of the relevant parameters are in appropriate ranges.

[55] A strong influence of αs was found even for configurations containing low abundances relative to protons such as ~2%, an abundance lower than that for the typical solar wind. In particular, the instability of EICWs depends strongly on the thermal anisotropy of alpha particles, a very poorly known parameter in ICMEs. Thus, we suggest that more exhaustive determinations of A_α are needed to allow us to study in more detail the activity of EICWs in ICMEs.

[56] Since the unstable frequency range is usually followed by a damping band with similar rate, non-local transport phenomena can occur in ICMEs. Waves that are amplified in a region of a ICME can be damped in another, if the parameters in each of these regions are the appropriate ranges.

[57] This paper has analyzed parallel propagation of EICWs on a homogeneous plasma. However, it is possible that other modes can be excited from the thermal anisotropy of ICMEs. For instance, recent studies [*Daughton and Gary*, 1998; *Voitenko and Goossens*, 2002] have shown that in some solar wind regimes (not ICME), and for appropriate parameters, oblique modes can have larger growth rates than the parallel EICW mode. Thus, studies considering linear stage but with non-parallel propagation can be done in order to decide whether these compete with RH-EICWs in the extraction of free energy from the plasma. Also, the propagation of Alfvén waves through non homogeneous helical magnetic configurations may be considered in order to gain more insight into the true role of EICWs in ICMEs.

[58] ICMEs are very non-uniform objects, and variations of the background plasma/magnetic field influence the wave characteristics and modify the wave dynamics. In particular, a cross-field inhomogeneity introduces wave phase mixing with an increase of the perpendicular component of the wave vector, bringing about harmonic ion-cyclotron resonances and other finite ion gyroradius effects. Again, a field-aligned inhomogeneity changes the parallel wave number, which can detune the wave from resonance, or even take it out of the unstable region.

[59] In addition, non-linear physical mechanisms of saturation for this instability have to be analyzed for ICMEs parameter regimes. Hybrid simulations can be proper to carry out this kind of analysis, due to the electrons do not resonate with this waves.

[60] To sum up, based on statistical works and some cases studied, our theoretical results show that some regions of ICMEs can sustain activity of right-hand polarized electromagnetic ion cyclotron waves.

Appendix A: Dispersion Relation for the κ Function Distribution Along the Field

[61] The dispersion relation for right-handed electromagnetic ion cyclotron waves propagating parallel to the magnetic field, can be expressed as $k^2c^2 = \omega^2\,\epsilon_R$. From kinetic theory, the dielectric constant for this waves, ϵ_R, can be expressed as

$$\epsilon_R = 1 + \sum_s \chi_s \tag{A1}$$

with the susceptibilities given by [e.g., *Stix*, 1992]

$$\chi_s = \pi\frac{\omega_{p,s}^2}{\omega^2}\left[\int_{-\infty}^{+\infty} dv_\parallel \int_0^\infty dv_\perp v_\perp^2 \cdot\frac{(\omega - kv_\parallel)\partial f/\partial v_\perp + kv_\perp \partial f/\partial v_\parallel}{\omega + \Omega_s - kv_\parallel}\right] \tag{A2}$$

where $f(v_\parallel, v_\perp)$ is the distribution function for the species s. When a component of minority suprathermal κ-protons with f as in equation (6) is considered, the susceptibility for this species, χ_κ, is given by

$$\chi_\kappa = -\frac{2\omega_{p,\kappa}^2}{\omega^2}\frac{\Gamma(\kappa+1)}{\Gamma(\kappa-1/2)\kappa^{3/2}\pi^{1/2}}\int_{-\infty}^{+\infty}\frac{dv_\parallel}{\theta_\parallel}\int_0^\infty \frac{dv_\perp}{\theta_\perp}\frac{v_\perp^2}{\theta_\perp^2} \cdot\left\{\frac{v_\perp}{\theta_\perp}\exp\left[-\frac{v_\perp^2}{\theta_\perp^2}\right]\frac{\omega - kv_\parallel}{\omega + \Omega_p - kv_\parallel}\left(1 + \frac{v_\parallel^2}{\theta_\parallel^2\kappa}\right)^{-\kappa} + \frac{k}{\theta_\perp\theta_\parallel^2}\frac{v_\perp}{\theta_\perp}\frac{\exp\left[-\frac{v_\perp^2}{\theta_\perp^2}\right]}{\omega + \Omega_p - kv_\parallel}\left(1 + \frac{v_\parallel^2}{\theta_\parallel^2\kappa}\right)^{-\kappa-1}\frac{v_\parallel}{\theta_\parallel}\right\} \tag{A3}$$

[62] Then, after an integration of $v_\perp$ and $v_\parallel$ (using the Landau's rule), it is possible to obtain,

$$\chi_\kappa = \frac{\omega_{p,\kappa}^2}{\omega^2}\left\{-1 + \frac{\kappa - 1/2}{\kappa - 3/2}(A_\kappa + 1) - \frac{\Omega_p}{k\theta_\parallel}\frac{(\kappa-1)^{3/2}}{\kappa^{1/2}(\kappa - 3/2)}Z_{\kappa-1} \cdot\left(\sqrt{\frac{\kappa-1}{\kappa}}\frac{\omega + \Omega_p}{k\theta_\parallel}\right) + \frac{\omega + \Omega_p}{k\theta_\parallel}\frac{\kappa}{\kappa - 3/2}(A_\kappa + 1)Z_\kappa\left(\frac{\omega + \Omega_p}{k\theta_\parallel}\right)\right\} \tag{A4}$$

[63] Finally, and using dimensionless variables, we can obtain,

$$\chi_\kappa = \frac{c^2}{x^2 v_{A,p}^2}\eta_\kappa\left\{-1 + \frac{\kappa - 1/2}{\kappa - 3/2}(A_\kappa + 1) - \left(\frac{\kappa - 1}{\kappa - 3/2}\right)^{3/2} \cdot\frac{1}{y\beta_{\parallel,\kappa}^{1/2}}Z_{\kappa-1}\left(\sqrt{\frac{\kappa-1}{\kappa - 3/2}}\frac{x+1}{y\beta_{\parallel,\kappa}^{1/2}}\right) + \left(\frac{\kappa}{\kappa - 3/2}\right)^{3/2} \cdot(A_\kappa + 1)\frac{x+1}{y\beta_{\parallel,\kappa}^{1/2}}Z_\kappa\left(\sqrt{\frac{\kappa}{\kappa - 3/2}}\frac{x+1}{y\beta_{\parallel,\kappa}^{1/2}}\right)\right\}, \tag{A5}$$

where the relationship $(\theta_\parallel/v_{A,p})^2 = \beta_{\parallel,\kappa}\frac{\kappa-3/2}{\kappa}$ has been used.

[64] Thus, for a plasma containing minority κ-protons, the dispersion relation include the term written in equation (9), section (2.2), which is directly derived from equation (A5).

[65] **Acknowledgments.** This work was partially supported by the Argentinian CONICET grant PIP4536/96, UBA grant UBACYT X059, USA NASA grant NAG5-11803, and NASA Living with a Star grant NAG5-10883. SD is a fellow of CONICET. SD would likes to thank to Cristina Mandrini for reading the manuscript and constructive remarks. The authors are grateful to both referees, whose constructive criticisms helped us to improve this paper.

[66] Shadia Rifai Habbal thanks Charles W. Smith, Marcel I. Goosens, and Yurii Voitenko for their assistance in evaluating this paper.

References

Bame, S. J., J. R. Asbridge, W. C. Feldman, J. T. Gosling, and R. D. Zwickl, Bi-directional streaming of solar wind electrons >80 eV: ISEE evidence for a closed field structure within the driver gas of an interplanetary shock, *Geophys. Res. Lett.*, *8*, 173–176, 1981.

Borrini, G., J. T. Gosling, S. J. Bame, and W. C. Feldman, Helium abundance enhancements in the solar wind, *J. Geophys. Res.*, *87*, 7370–7378, 1982.

Burlaga, L. F., *Interplanetary Magnetohydrodynamics*, 248 pp., Oxford Univ. Press, New York, 1995.

Burlaga, L. F., E. Sittler, F. Mariani, and R. Schwenn, Magnetic loop behind an interplanetary shock: Voyager, Helios, and IMP 8 observations, *J. Geophys. Res.*, *86*, 6673–6684, 1981.

Burlaga, L. G., et al., A magnetic cloud containing prominence material: January 1997, *J. Geophys. Res.*, *103*, 277–285, 1998.

Dasso, S., F. T. Gratton, and C. J. Farrugia, The influence of proton thermal properties on electromagnetic ion cyclotron wave activity in solar ejecta, in *Solar Wind Nine*, edited by S. Habbal et al., *AIP Conf. Proc.*, *471*, 669–672, 1999.

Dasso, S., F. T. Gratton, C. J. Farrugia, and G. Gnavi, The influence of electron thermal properties on the instabilities of right hand polarized cyclotron waves in coronal mass ejections, in *The Solar Wind-Magnetosphere System 3*, edited by H. K. Biernat, C. J. Farrugia, and D. F. Vogl, pp. 71–80, Austrian Acad. of Sci. Press, Vienna, 2000.

Dasso, S., C. J. Farrugia, F. T. Gratton, R. P. Lepping, K. W. Ogilvie, and R. Fitzenreiter, Waves in the proton cyclotron frequency range in the coronal mass ejection observed by Wind on August 7–8, 1996: Theory and data, *Adv. Space Res.*, *28*(5), 747–752, 2001.

Dasso, S., F. T. Gratton, and C. J. Farrugia, The role of alpha particles in the emission of plasma waves inside solar ejecta, *Braz. J. Phys.*, *32*(2B), 632–635, 2002.

Daughton, W., and P. S. Gary, Electromagnetic proton/proton instabilities in the solar wind, *J. Geophys. Res.*, *103*, 20,613–20,620, 1998.

Farrugia, C. J., F. G. Gratton, G. Gnavi, and K. W. Ogilvie, On the possible excitation of electromagnetic ion cyclotron waves in solar ejecta, *J. Geophys. Res.*, *103*, 6543–6550, 1998a.

Farrugia, C. J., et al., Geoeffectiveness of three Wind magnetic clouds: A comparative study, *J. Geophys. Res.*, *103*, 17,261–17,278, 1998b.

Galvin, A. B., Minor ion composition in CME-Related Solar Wind, in *Coronal Mass Ejections*, *Geophys. Monogr. Ser.*, vol. 99, edited by N. Crooker, J. A. Joselyn, and J. Feynman, pp. 253–260, AGU, Washington, D. C., 1997.

Galvin, A. B., F. M. Ipavich, G. Gloeckler, D. Hovestadt, S. J. Bame, B. Klecker, M. Scholer, and B. T. Tsurutani, Solar wind charges states preceding a driver plasma, *J. Geophys. Res.*, *92*, 12,069–12,081, 1987.

Gary, S. P., *Theory of Plasma Microinstabilities*, Cambridge Univ. Press, New York, 1993.

Gosling, J. T., Coronal mass ejections and magnetic flux ropes in interplanetary space, in *Physics of Magnetic Flux Ropes*, *Geophys. Monogr. Ser.*, vol. 58, edited by C. T. Russell, E. R. Priest, and L. C. Lee, pp. 343–364, AGU, Washington, D. C., 1990.

Gosling, J. T., J. R. Asbridge, S. J. Bame, W. C. Feldman, and R. D. Zwickl, Interplanetary ions during an energetic storm particles event: The distribution function from solar wind thermal energies to 1.6 MeV, *J. Geophys. Res.*, *86*, 547–554, 1981.

Gosling, J. T., D. N. Baker, S. J. Bame, W. C. Feldman, and R. D. Zwickl, Bidirectional solar wind electron heat events, *J. Geophys. Res.*, *92*, 8519–8535, 1987.

Gratton, F. T., S. Dasso, and C. J. Farrugia, Electron and alpha particle influence on the excitation of right hand polarized electromagnetic ion cyclotron waves in solar ejecta, in *Proceedings of 1998 International Congress on Plasma Physics & 25th European Physical Society Conference on Controlled Fusion and Plasma Physics, Praha*, edited by P. Pavlo, ECA, *Eur. Phys. Soc.*, *22C*, 1122–1125, 1998.

Kennel, C. F., and F. L. Scarf, Thermal anisotropies and electromagnetic instabilities in the solar wind, *J. Geophys. Res.*, *73*, 6149–6165, 1968.

Marsch, E., Kinetic physics of the solar wind plasma, in *Physics of the Inner Heliosphere II*, edited by R. Schwenn and E. Marsch, pp. 45–133, Springer-Verlag, New York, 1991.

Marsden, R. G., T. R. Sanderson, C. Tranquille, K.-P. Wenzel, and E. J. Smith, ISEE 3 observations of low-energy proton bidirectional events and their relation to isolated interplanetary structures, *J. Geophys. Res.*, *92*, 11,009–11,019, 1987.

Montgomery, M. D., J. R. Asbridge, S. J. Bame, and W. C. Feldman, Solar wind electron temperature depressions following some interplanetary shock waves: Evidence for magnetic merging?, *J. Geophys. Res.*, *79*, 3103, 1974.

Neugebauer, M., and R. Goldstein, Particle and field signatures of coronal mass ejections in the solar wind, in *Coronal Mass Ejections*, *Geophys. Monogr. Ser.*, vol. 99, edited by N. Crooker, J. A. Joselyn, and J. Feynman, 245 pp., AGU, Washington, D. C., 1997.

Osherovich, V., and L. F. Burlaga, Magnetic clouds, in *Coronal Mass Ejections*, *Geophys. Monogr. Ser.*, vol. 99, edited by N. Crooker, J. A. Joselyn, and J. Feynman, pp. 157–168, AGU, Washington, D. C., 1997.

Osherovich, V. A., C. J. Farrugia, L. F. Burlaga, R. P. Lepping, J. Fainberg, and R. G. Stone, Polytropic relationship in interplanetary magnetic clouds, *J. Geophys. Res.*, *98*, 15,331–15,342, 1993.

Pillipp, W. G., H. Miggenrieder, M. D. Montgomery, K. H. Muhlhauser, H. Rosenbauer, and R. Schwenn, Unusual electron distribution functions in the solar wind derived from the Helios Plasma Experiment: Double-Strahl distributions and distributions with an extremely anisotropic core, *J. Geophys. Res.*, *92*, 1093–1101, 1987.

Richardson, I. G., and H. V. Cane, Regions of abnormally low proton temperature in the solar wind (1965–1991) and their association with ejecta, *J. Geophys. Res.*, *100*, 23,397–23,412, 1995.

Richardson, I. G., C. J. Farrugia, and H. V. Cane, A statistical study of the behavior of the electron temperature in ejecta, *J. Geophys. Res.*, *102*, 4691–4700, 1997.

Schwenn, R., Large-scale structure of the interplanetary medium, in *Physics of the Inner Heliosphere I*, edited by R. Schwenn and E. Marsch, pp. 99–181, Springer-Verlag, New York, 1990.

Stix, T. H., *Waves in Plasmas*, AIM, New York, 1992.

Summers, D., and R. M. Thorne, The modified plasma dispersion function, *Phys. Fluids*, *B3*(8), 1835–1847, 1991.

Summers, D., and R. M. Thorne, A new tool for analyzing microinstabilities in space plasmas modeled by a generalized Lorentzian (Kappa) distribution, *J. Geophys. Res.*, *97*, 16,827–16,832, 1992.

Treumann, R. A., and W. Baumjohann, *Advanced Space Plasma Physics*, Imperial Coll. Press, London, 1977.

Voitenko, Y., and M. Goossens, Excitation of high-frequency Alfvén waves by plasma outflows from coronal reconnection events, *Sol. Phys.*, *206*, 285–313, 2002.

Xue, S., and R. M. Thorne, Electromagnetic ion-cyclotron instability in space plasmas, *J. Geophys. Res.*, *98*, 17,475–17,484, 1993.

Zwickl, R. D., J. R. Asbridge, S. J. Bame, W. C. Feldman, J. T. Gosling, and E. J. Smith, Plasma properties of driver gas following interplanetary shocks observed by ISEE 3, in *Solar Wind Five*, *NASA Conf. Publ.*, *CP-2280*, 711–717, 1983.

S. Dasso, Instituto de Astronomía y Física del Espacio (IAFE), CC 67 Suc. 28, 1428 Buenos Aires, Argentina. (dasso@df.uba.ar)

C. J. Farrugia, Institute for the Study of Earth, Oceans, and Space, Space Science Center, University of New Hampshire, Morse Hall, Durham, NH 03824, USA. (charlie.farrugia@unh.edu)

F. T. Gratton, Instituto de Física del Plasma, Departamento de Física FCEyN/UBA-CONICET, Ciudad Universitaria, Pab.1, Buenos Aires 1428, Argentina. (faustogratton@infip.org)